Geophys. J. Int. (1994) **117**, 205–222

The structure of the Nazca ridge and Sala y Gomez seamount chain from the dispersion of Rayleigh waves

Mark T. Woods and Emile A. Okal
Department of Geological Sciences, Northwestern University, Evanston, Illinois 60208, USA

Accepted 1993 September 6. Received 1993 August 25; in original form 1993 February 16.

SUMMARY

We report single-station measurements of group velocity for fundamental mode Rayleigh waves that propagated along two 'aseismic ridges' in the eastern Pacific Ocean basin: the Nazca ridge and the Sala y Gomez chain. We find that the Nazca ridge dispersion curves, when regionalized to isolate the ridge contribution, indicate group velocities of about 3.5 km s^{-1} for short periods. These values are slower than predicted for the geometry of the propagation paths. Interpreting this velocity heterogeneity is complicated by the recognition that the Nazca ridge is about 1000 km longer than previously thought, but models of V_{SV} for the ridge derived by inverting the dispersion curves reveal abnormally thick (18 ± 3 km) oceanic crust along its longitudinal axis. This value compares favourably with previously published results over the Tuamotu plateau, thus strengthening the hypothesis that the Nazca ridge and Tuamotu plateau are mirror images, formed by a hotspot coincident with the Farallon–Pacific spreading centre before 20 Ma. In contrast, the measurements along the Sala y Gomez chain are consistent with typical oceanic crust and mantle. When these values are inverted, they reveal no thick crust (6 km) along the Sala y Gomez chain. We conclude from this result that the chain was likely formed as a leaky fracture zone, not as a simple hotspot track.

Key words: aseismic ridges, crustal structure, Rayleigh wave dispersion.

INTRODUCTION

Since the seminal work of Wilson (1963a, 1963b, 1963c) it has been thought that oceanic plateaus and 'aseismic ridges' are formed when hotspot plumes coincide with active spreading centres. Many such structures are found in the southeastern Pacific Ocean basin, and two of these, the Nazca ridge and the Sala y Gomez seamount chain, are the topic of this paper. We have investigated the crustal thickness and upper mantle velocity structure along these bathymetric features using the geometric dispersion of Rayleigh waves, for with the continued interest in the nature of mantle plumes (e.g. Sleep 1992), especially in their interaction with oceanic lithosphere, it seems beneficial to put the tightest constraints possible on observable surface structures that are thought to result from plume action.

Many studies have demonstrated that other aseismic plateaus and ridges are underlain by anomalously thick crust. For example, Talandier & Okal (1987) determined that the crustal thickness of the Tuamotu plateau on the Pacific plate is about 22–27 km, comparable with that found in Iceland and along the Iceland–Faeroe ridge (e.g. Båth 1960; Tryggvason 1962; Bott & Gunnarsson 1980). This result is significant for the present study because the Tuamotu plateau is the mirror image of the Nazca ridge in various reconstructions of the kinematic evolution of the Nazca (Farallon)–Pacific spreading centre (e.g. Herron 1972; Morgan 1972; Handschumacher 1976; Okal & Cazenave 1985). If these two edifices were indeed formed by a single hotspot coincident with the spreading centre, a similar crustal thickness along the Nazca ridge might be expected. Expectations of thick crust along the Sala y Gomez chain are less sure; it has no clear mirror image edifice on the Pacific plate. Moreover, several reconstructions are incompatible with the hypothesis that it is a simple hotspot track (e.g. Pilger & Handschumacher 1981).

Previous attempts at determining the crustal thickness along these structures with refraction sonobuoy arrays have yielded mixed results. Principal (1974) found no clear evidence of abnormally thick crust along the Sala y Gomez chain, and she concluded that it is at most 8 km. Cutler (1977), however, found that the thickness along the Nazca ridge may be 13 km or more. Given that both surveys employed only a few profiles perpendicular to the

structures, these results may reflect only local conditions. The dispersion of seismic surface waves in the period range $15 \leq T \leq 80$ s, with their ability to sample to depths of ~100 km, provides a suitable probe of the ridges' average velocity structures along their longitudinal axes. Knowing their average structures might then allow us to place bounds on the hotspot's volcanic production rate, which in turn could help constrain models of the heat and mass flux of mantle plumes.

It is important to note that these structures are large, with lengths of about 1200 km for the Nazca ridge, and about 2500 km for the Sala y Gomez chain. Thus, if the oceanic crust is indeed abnormally thick along their longitudinal axes, they should represent significant lateral heterogeneities in the distribution of group and phase velocities within the Pacific basin. Nevertheless, they do not appear in currently available tomographic images of the basin for several reasons. Crustal thickness affects most strongly the shortest

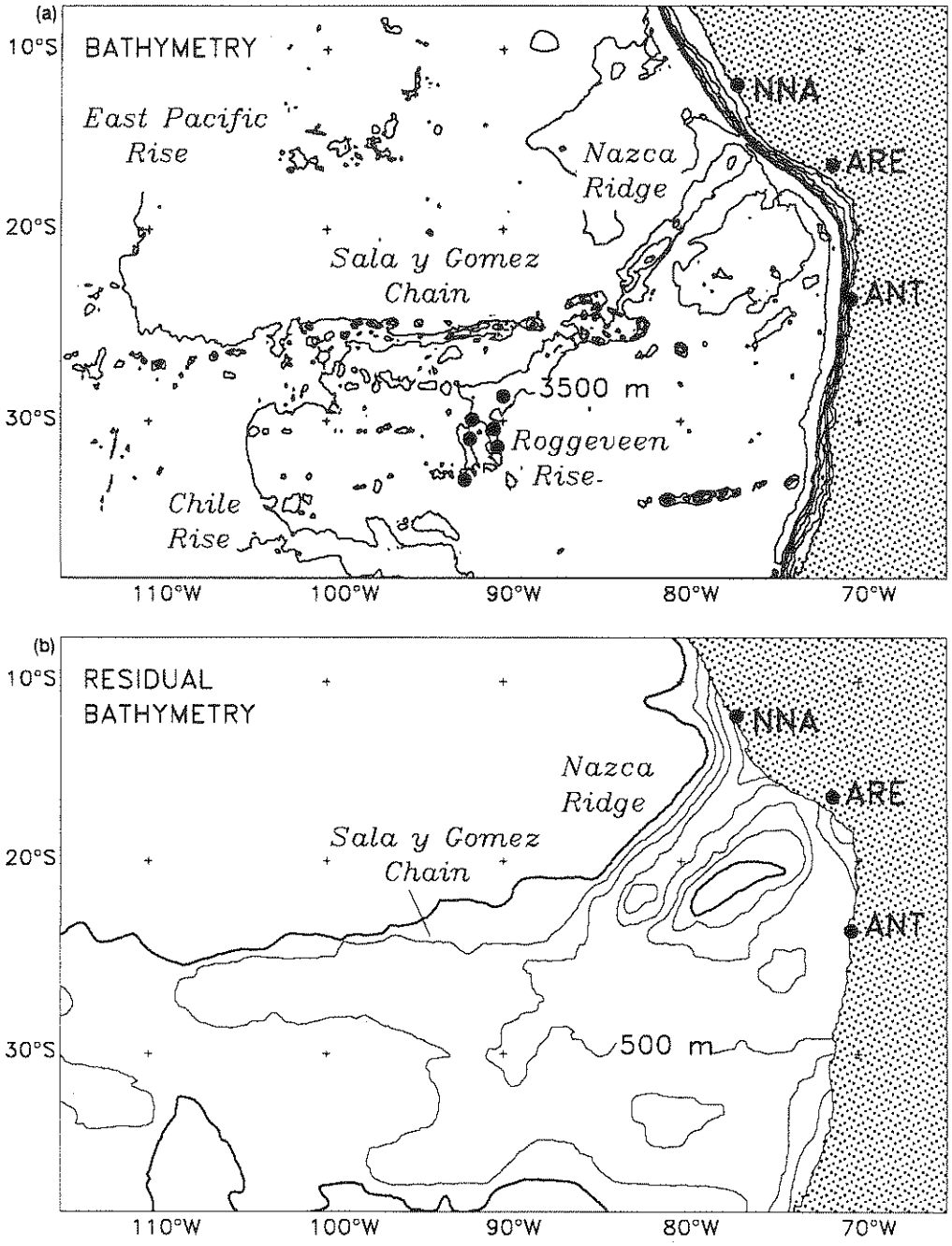

Figure 1. (a) Map (Mercator projection) of DBDB5 bathymetry over study area. Contour interval is 1000 m beginning at 500 m. Clearly visible are the Nazca ridge and the Sala y Gomez chain. Note also the extension of the 3500 m isobath from the Nazca ridge to the extinct Roggeveen rise. The filled circles on the Roggeveen rise represent verified intraplate earthquake epicentres. (b) Map (Mercator projection) of residual bathymetry over study area. Contour interval is 250 m; heavy contour is 0 m residual. The Nazca ridge and its proposed extension are visible as 500 m isobath. The Sala y Gomez chain is contained by the 250 m isobath. Note also that much of the Nazca plate between 25°S and 35°S is anomalously shallow.

periods ($10 \leq T \leq 20$ s) of dispersed Rayleigh and Love wave trains. Nishimura & Forsyth's (1988) 20 s Rayleigh wave phase velocities should have sampled the structures adequately, but the path coverage was not sufficiently dense to resolve them. In contrast, the dense path coverage of Zhang & Tanimoto (1989, 1991) is more than enough to image the structures, but their data, with $75 \leq T \leq 250$ s, sampled only the upper mantle. Detailed regional-scale studies, such as those we present here, supplement global-scale tomographic work by sharpening the details of the velocity distributions.

BATHYMETRIC SETTING

Examination of the bathymetry of the Nazca ridge and Sala y Gomez chain raises several questions about the length and breadth of the target structures, and thus their roles in the evolutionary history of the Nazca plate. Fig. 1(a) illustrates DBDB5 digital bathymetric data (U.S. Naval Oceanographic Office 1985) over the study area, contoured with a 1000 m interval, and beginning at a depth of 500 m. The Nazca ridge is clearly visible, being about 300 km wide at its base, standing about 1.5 km above the surrounding abyssal plain, and extending south-west from the Chile trench to where it intersects the Sala y Gomez chain at about 24°S, 83°W. This intersection is characterized by a zone of rugged bathymetry, roughly oval in shape. Past the intersection, however, the 3500 m isobath continues south-west to about 29°S, 90°W, thereby forming a linear feature of low relief along the same geographic trend as the recognized Nazca ridge. The extension appears to terminate at the relict Roggeveen rise, which was abandoned in a plate reorganization at about 20 Ma (Mammerickx, Herron & Dorman 1980), and where six intraplate earthquakes (shown as filled circles) have occurred (Wysession, Okal & Miller 1991). The extension is also visible in the 500 m contour of the residual depth map (Fig. 1b) constructed by Smith (1990). To the best of our knowledge, this feature has never been recognized or discussed in any evolutionary scenario for the Farallon–Nazca–Pacific plate system. We therefore propose that the Nazca ridge indeed extends to the Roggeveen rise, so that it is nearly twice as long as previously thought (e.g. Handschumacher 1976; Pilger & Handschumacher 1981). Implications of this hypothesis will be discussed later. Thus, for the interpretation of on-ridge Rayleigh wave dispersion in this investigation, we shall consider two cases: a short Nazca ridge, and a long Nazca ridge.

Contrasted with the massive edifice of the Nazca ridge, the Sala y Gomez chain consists of small, disconnected and elongated seamounts sitting atop a narrow ridge delineated by the 3500 m isobath. It is best defined in the DBDB5 bathymetry along 25°S between about 87°W and 100°W, where it merges with a broader swell extending eastward from the East Pacific rise. Astride this swell are Sala y Gomez Island, Easter Island, and several small seamounts. Connecting the broad swell with the Roggeveen rise is a line of closed 3500 m isobaths, presumed to be seamounts. If the Nazca ridge indeed extended to the Roggeveen rise, then these seamounts may be remnants of the Pacific-side mirror image. Therefore they, not the Sala y Gomez chain, trace

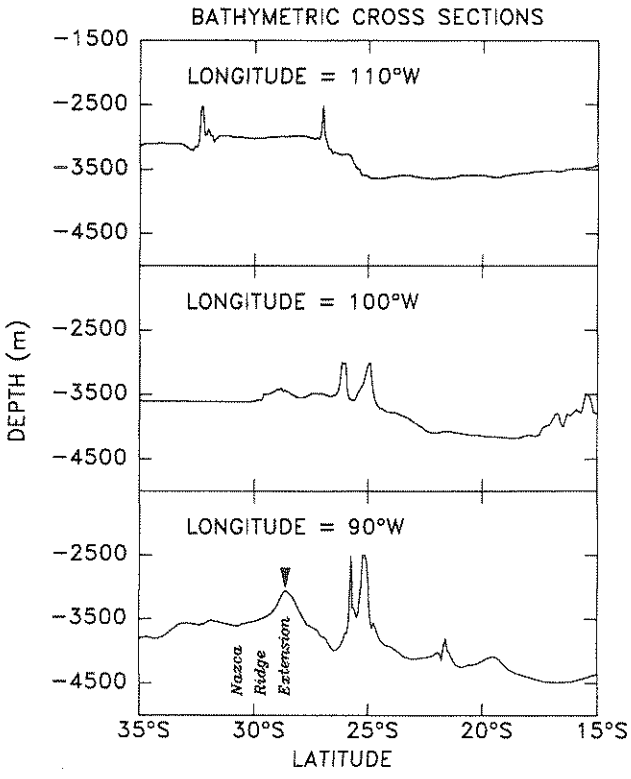

Figure 2. Bathymetric cross-sections of the Sala y Gomez chain constructed from DBDB5 data along three longitudes. Note the narrow width (~100 km) of the Sala y Gomez chain, the proximity of the Easter fracture zone (the 500 m discontinuity in depth at 25°S), and the appearance of the proposed extension to the Nazca ridge.

the Pacific-hotspot motion. Neither these unnamed seamounts nor the Sala y Gomez chain are visible on the map of residual bathymetry because they are so small. They are enclosed, however, by the 250 m contour between 90°W and 110°W.

The narrow width of the Sala y Gomez chain is particularly clear when the bathymetry is examined in cross-section. Fig. 2 presents three representative cross-sections, at longitudes 90°W, 100°W and 110°W. In two of these figures, the chain is double peaked, with a deep between two highs. This feature is repeated in other cross-sections that are not illustrated. The width of the chain ($\leq$100 km) is a potential problem for investigating its structure with surface waves, because it approaches the wavelengths to be used. Another potential problem is that the chain lies on the northern edge of a depth discontinuity in the ocean floor. Sometimes identified as the Easter fracture zone, the discontinuity is sharpest in the westernmost cross-section, where the ocean floor appears to be about 500 m deeper north of latitude 25°S. Surface waves propagating along such a discontinuity may be scattered or refracted laterally, and thus deviated from the ideal great circle propagation path.

DATA SELECTION AND ANALYSIS

Selection of propagation paths

For this study we used Rayleigh waveforms generated by 31 earthquakes along the East Pacific rise and the Chile rise, and recorded by the WWSSN stations ANT, ARE, and NNA. The propagation paths are illustrated in Fig. 3, where for clarity only schematic outlines of the targeted structures are shown. The paths crossing the Nazca ridge do a fair job of sampling the structure; roughly one fourth to one third of each path is over the ridge. The paths traversing the Sala y Gomez chain do not sample it as well. The southernmost paths merely graze the southern margin of the seamount chain. They do sample, however, the broader Sala y Gomez structure visible in the 250 m residual isobath.

Because seismograph stations are situated only on the South American coast, only single-station velocity measurements can be made. Two-station measurements, in which instruments are located at either end of the target structure, are not possible. Thus, to isolate the contributions of the aseismic ridges, we must make a two-province, pure-path regionalization of the measurements. Presumed normal crust and mantle are represented by the paths to stations ARE and ANT in the Nazca ridge suite; no such paths are used in Sala y Gomez suite.

The hypocentres obtained from the NEIC and ISC catalogues for the earliest of these earthquakes routinely listed the focal depths as 33 km, too deep for earthquakes along divergent and transform plate boundaries. A more appropriate value is 10 km, a lower limit along such boundaries which can be explained in terms of their rapidly evolving, temperature-dependent rheological properties (see Stein & Wiens (1986) for a review of the relevant literature). We therefore relocated each earthquake with the focal depth fixed at this value using arrival times culled from the Bulletin of the International Seismological Centre. Table 1 lists the revised epicentres used in the present study. For the Nazca ridge suite, the relocation vectors averaged 34.3 ± 16.4 km at a mean azimuth of $310 \pm 39°$. The revised origin times averaged 2.90 ± 1.35 s earlier than published. For the Sala y Gomez suite the average relocation vector was 21.1 ± 10.5 km with a mean azimuth slightly more to north, at $352 \pm 27°$. The revised origin times averaged 0.22 ± 0.50 s later than published. As discussed by Forsyth (1975), had the epicentres remained systematically southeast and south of their actual locations, velocities measured over paths from west to east would have appeared to be anomalously slow, and velocities measured from south to north would have been anomalously fast. By first relocating the epicentres we removed this bias, which would have been interpreted erroneously as azimuthal anisotropy.

The listed earthquakes occurred on the spreading axis of either the East Pacific rise or the Chile rise, or on transform

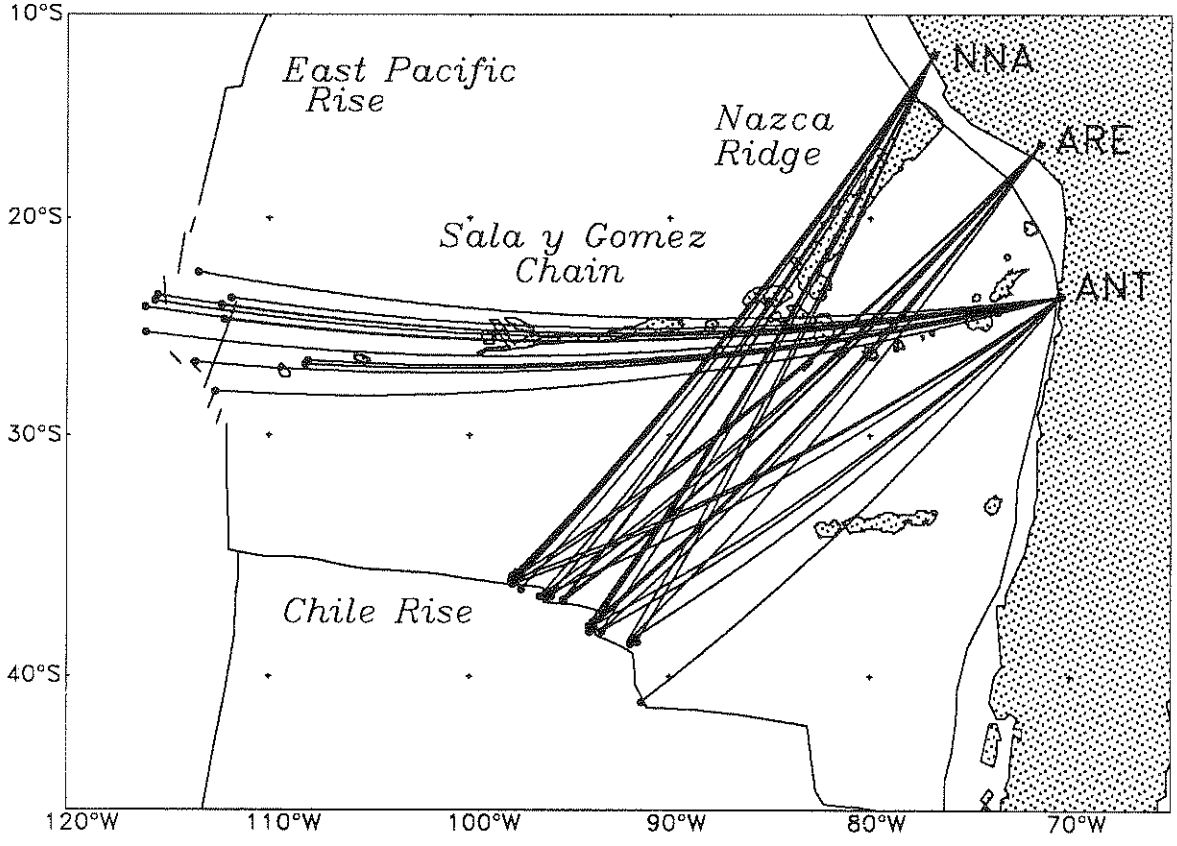

Figure 3. Map (Mercator projection) illustrating the propagation paths used in this study. The Nazca ridge suite consists of paths from earthquakes on the Chile rise to the WWSSN stations ANT, ARE and NNA. The ARE and ANT waveforms provide an off-ridge comparison with the on-ridge NNA data. The Sala y Gomez suite consists of paths from events on the East Pacific rise to ANT only. Note that the sampling of the Nazca ridge is more complete than for the Sala y Gomez chain.

Table 1. Revised earthquake locations with 10 km focal depths.

No.	Date	Origin Time U.T.C.	Lat. (° S)	Lon. (° W)	σ_{RMS} (s)	M_s
		Nazca Ridge Suite				
1	1965 Jun 25	20:26:59.5	36.95	96.14	1.10	5.3*
2	1965 Sep 12	20:21:16.4	36.18	97.95	1.00	5.4*
3	1965 Sep 13	16:15:41.5	36.35	97.83	1.78	5.4*
4	1966 Jul 18	22:15:35.3	38.11	94.00	0.97	5.1*
5	1966 Nov 24	16:45:42.8	38.71	92.15	1.89	5.1*
6	1967 Feb 22	03:51:11.9	36.55	97.43	0.92	5.0*
7	1970 Jun 17	21:30:12.1	36.28	97.89	1.60	5.5
8	1970 Dec 13	23:08:19.3	40.99	91.44	1.32	5.0*
9	1972 Jun 18	00:58:31.3	36.96	95.32	1.10	5.0
10	1972 Jun 18	01:00:40.5	37.05	95.30	1.14	5.5
11	1972 Oct 08	02:45:38.6	38.27	93.45	1.08	5.1
12	1972 Dec 29	06:47:39.6	35.83	97.63	1.78	5.4
13	1974 Apr 18	20:32:58.3	38.04	93.79	1.04	4.7
14	1974 Apr 18	21:05:55.1	38.04	94.05	1.24	4.7
15	1975 Feb 08	02:05:42.3	36.83	96.45	1.49	5.1
16	1976 Nov 25	20:24:26.5	38.71	91.66	1.26	5.5
17	1978 Mar 18	07:09:28.9	37.81	93.90	1.33	5.0
18	1978 Mar 18	09:13:11.2	37.99	93.97	1.19	5.6
19	1979 Jun 10	06:32:52.0	36.02	97.89	1.42	6.0
		Sala y Gomez Suite				
1	1979 May 10	02:09:50.6	23.77	111.88	1.82	4.9
2	1979 May 10	07:15:55.3	24.12	112.34	0.90	4.7
3	1980 Nov 24	09:33:05.1	22.58	113.50	0.98	5.4
4	1984 Mar 27	20:51:37.5	23.64	115.51	1.14	5.6
5	1984 Apr 13	05:54:51.6	24.77	112.24	0.77	4.8
6	1984 Sep 05	22:27:54.7	25.35	116.11	1.35	5.4
7	1985 Nov 27	00:32:33.6	23.91	115.63	1.19	4.7
8	1987 Jul 06	01:06:08.7	26.81	108.24	1.40	6.3
9	1987 Jul 08	11:50:15.3	26.65	108.10	0.68	5.9
10	1988 May 05	22:32:49.5	26.71	113.66	1.20	5.9
11	1988 Jul 30	02:45:14.0	24.20	116.12	1.58	5.3
12	1988 Aug 10	11:46:47.3	28.03	112.67	1.08	5.9

* *Unified magnitude*

faults, so they likely result from either normal or strike-slip fault motion. The earthquakes were, however, only moderately sized, so it was not possible to construct reliable focal mechanisms from either first-motion polarities or from surface-wave radiation patterns. Accurate source phases ϕ_s are therefore unknown, and so single-station measurements of phase velocity would be strongly biased by the assumed ϕ_s values. We therefore rely on measurements of group velocity only.

Group velocity analysis

After digitizing the analogue waveforms, we computed their amplitude spectra, and removed the instrument responses. Group velocities were then calculated from the corrected spectra in two ways. First, we applied multiple-filter analysis (MFA) (e.g. Dziewonski & Hales 1972; Herrmann 1973) to establish the gross dispersion characteristics of the individual spectra. To eliminate the interference

effects of multipath propagation, we also performed velocity analyses with phase match filters (PMF) (Herrin & Goforth 1977), using the variable-frequency windows advocated by Russell, Herrmann & Hwang (1988) and allowing for a 10 per cent bias in the amplitude spectrum. The PMF extract fundamental mode signals with smooth spectra so that the levels of incoherent noise are reduced; increases in the signal-to-noise ratio were as large as 120 dB. The results from the two techniques were consistent with one another, but the MFA values were considerably more scattered because of the cumulative effects of small signal-to-noise ratios, the trade-off between resolutions in the time and frequency domains for the Gaussian filters, and multipathing. We therefore prefer to use the PMF group velocities, which are presented below.

GROUP VELOCITY RESULTS

Nazca ridge suite

The group velocities measured at the stations ANT, ARE, and NNA from the Nazca ridge suite were averaged by station, and are presented in Fig. 4(a) to illustrate the general features of the dispersion off and on the ridge. Although there is some overlap of the standard errors for $T \leq 35$ s, it is clear that the maximum velocities observed at NNA for paths intersecting the ridge are only ~3.9 km s^{-1}, or about 2.5 per cent slower than at ANT and ARE (~4.0 km s^{-1}). Moreover, in the period range most sensitive to the crustal velocity structure ($15 \leq T \leq 20$ s), the NNA values are 3–5 per cent slower than observed at the other two stations. Some of this difference can be attributed to the anisotropic fabric of the oceanic lithosphere. Because the fast *a*-axes of olivine crystals [100] in the crustal and upper mantle rocks of the lithosphere are expected to be parallel to the direction of sea-floor spreading, propagation paths in this direction should yield velocities that are about 1.5–2 per cent faster than do paths perpendicular to the spreading direction (Forsyth 1975; Yu & Mitchell 1979; Mitchell & Yu 1980; Nishimura & Forsyth 1988, 1989). However, because the maximum difference in propagation azimuths in this study is 26° we would expect only about 0.6 per cent difference in the measured group velocities.

Sala y Gomez suite

The group velocities measured for paths that intersect the Sala y Gomez chain were also averaged, and are illustrated in Fig. 4(b). Although only one station, ANT, was used, three average curves are shown; the solid circles represent the mean of all observations at each frequency. Observations appeared, however, to group into two populations with maximum values of 3.98 ± 0.01 and 3.93 ± 0.01 km s^{-1}, so averages of the subgroups are also shown. The differences between the subgroups cannot be attributed to anisotropy because the propagation azimuths for all paths are nearly constant; they average $97.2 \pm 2.6°$. It is, however, difficult to interpret the velocity differences in terms of on-ridge or off-ridge propagation because of the discontinuous nature of the Sala y Gomez chain, and especially the proximity of the Easter fracture zone. The four paths with significant fractions north of the fracture zone perhaps exhibit faster group velocities because they sample older lithosphere. Regardless, in the period range most sensitive to crustal structure ($15 \leq T \leq 20$ s) all three curves exhibit similar group velocities, with a minimum about 3.7 km s^{-1}. This value does not suggest abnormally thick oceanic crust anywhere along the propagation paths.

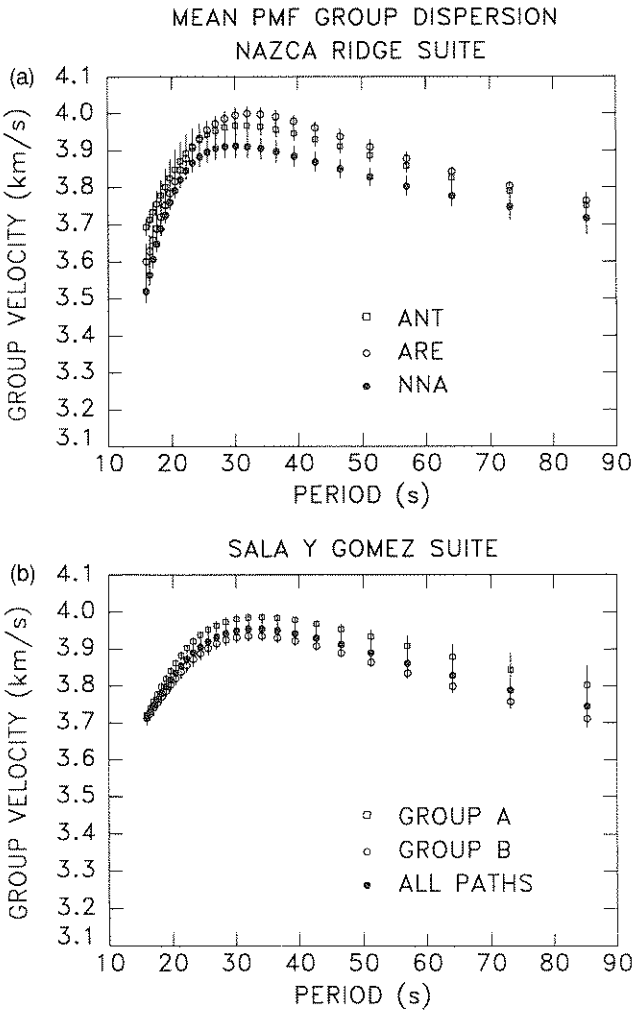

Figure 4. Summary of measured group velocity dispersion. (a) Nazca ridge suite; values represent means computed for all observations at a single station. (b) Sala y Gomez suite; values represent means computed for all paths, and for two subgroups of paths as discussed in text. Error bars represent two standard deviations. Note: all dispersion curves illustrated in this paper will use these velocity and period scales to facilitate comparison.

PURE-PATH REGIONALIZATION

To assess the contributions of the aseismic ridges to the observed dispersion curves, we applied the sequential pure-path technique. As outlined by Forsyth (1975) and Nishimura & Forsyth (1988, 1989) the pure-path delay t_i^{PP} along a great circle propagation path i is the sum of two terms:

$$t_i^{PP} = t_i^{aa} + t_i^{lh}, \quad (1)$$

where t_i^{aa} represents the contribution from the well-understood dependence on age and anisotropy, and t_i^{lh} represents the unknown contribution from lateral heterogeneity.

The first term of the right-hand side in eq. (1) is the sum of contributions through distinct age zones:

$$t_i^{aa} = \sum_{j=1}^{m} \frac{L_{ij}}{U_j}, \tag{2}$$

where L_{ij} is the length of the ith path in the jth age zone, and U_j is the anisotropic group velocity in the jth age zone. It is important to note that the anisotropic nature of U_j leads to a non-linear problem. Smith & Dahlen (1973) showed that group (and phase) velocity is a function of the average propagation azimuth θ:

$$U = U_0 + a\cos 2\theta + b\sin 2\theta + c\cos 4\theta + d\sin 4\theta. \tag{3}$$

Forsyth (1975) argued that path coverage is usually insufficient to resolve the 4θ terms in eq. (3), so they may be neglected. If the azimuthal dependence is then assumed to be weak ($U_0 \gg a, b$) and uniform throughout the region of study, t_i^{aa} becomes

$$t_i^{aa} = \sum_{j=1}^{m} \left(\frac{1}{U_j}\right) L_{ij} - \left(\frac{a}{U_0}\right) \frac{L_i\langle\cos 2\theta_i\rangle}{U_i^{obs}} - \left(\frac{b}{U_0}\right) \frac{L_i\langle\sin 2\theta_i\rangle}{U_i^{obs}}, \tag{4}$$

and inverting velocity observations for pure-path values becomes a linear problem in $1/U_j$, a/U_0 and b/U_0.

The second term of the right-hand side in eq. (1) is also a summation, being over the zones of lateral heterogeneity:

$$t_i^{lh} = \frac{-1}{U^2} \sum_{k=1}^{n} \delta U_k L_{ik}, \tag{5}$$

where δU_k is the group velocity perturbation in the kth anomalous zone, and L_{ik} is the length of the ith path in the kth anomalous zone.

Two sets of age-dependent velocities and anisotropy coefficients available in the literature are inadequate for application in eqs (1)–(5). Forsyth's (1975) values for the eastern Pacific are obsolete because the magnetic isochron maps used to parameterize the plate ages and the Euler poles to which the anisotropy coefficients were referenced have been revised. Nishimura & Forsyth's (1989) expanded results for the Pacific basin incorporate more recent age regionalizations and relative motion Euler poles, but tabulate only phase velocities.

Because pure-path group velocities are required in this investigation, we first inverted Forsyth's (1975) observed data set (whose sampling of the Nazca ridge was checked to be insignificant), to obtain revised pure-path values using a new age map of the ocean basin (Acton & Petronotis 1991). Based on the recent compilation of magnetic isochrons by Cande *et al.* (1989), this map is similar to the one by Larson *et al.* (1985), but differs in detail from the map of Sclater *et al.* (1981). For calculation of the propagation azimuths in a plate-kinematic reference frame, we used Euler poles for major plates of young lithosphere from the NUVEL-1 model (DeMets *et al.* 1990). For older lithosphere formed at the Farallon–Pacific (Far–Pac) spreading centre, we averaged poles for Chrons 7–13 (Pardo-Casas & Molnar 1987), and for relative motions between the Easter microplate and its neighbours we used the poles reported by Engeln & Stein (1984). Thus, an internally consistent set of pure-path group velocities and anisotropy coefficients was obtained with which we can model the group velocities reported above. The age-dependent group velocities obtained from this regionalization and inversion differ only slightly from those originally obtained by Forsyth. The coefficients of anisotropy differ significantly, however, primarily because of the addition of the Far–Pac Euler pole.

Nazca ridge suite

To determine quantitatively whether the difference between off- and on-ridge velocities can be explained by azimuthal anisotropy, we regionalized the measurements using eqs (1)–(5), and considered the two cases of a short and a long Nazca ridge. Using the new set of pure-path group velocities and anisotropy coefficients, we computed the group velocities that would be expected at ANT, ARE and NNA. These results are shown in Fig. 5(a). As expected, differences in the age dependence and azimuth are too small to account for the actual differences observed in the measured dispersion curves. For the shortest periods, the model group velocities are in the range of 3.7–3.9 km s^{-1}, which agrees reasonably well with the measurements at ANT and ARE. The range disagrees with the measurements at NNA, however, where values of about 3.5–3.7 km s^{-1} were obtained. We conclude from this difference that the velocity structure of the Nazca ridge severely retards short-period surface waves, most probably by a very thick crust. Most surprising is that the pure-path model curves for ANT and ARE in the period range $20 \le T \le 55$ s are significantly lower than was measured. For example, the model curves indicate that U_{max} at ANT should be about 3.95 km s^{-1}, and that both ARE and NNA values should be about 3.9 km s^{-1}. We observed, however, that ARE values are fastest, with $U_{max} \sim 4.0$ km s^{-1}, and that the ANT values are slightly less, ~3.95 km s^{-1}. Thus, the fastest group velocities in this vicinity occur along a direction about 15°N of the fossil plate motion.

To make this pattern more clear, we graph the average velocity residuals $\delta U = U_{obs} - U_{mdl}$ in Fig. 5(b). With this definition, positive residuals result when measured velocities are faster than the model values. Here, the most conspicuous residuals are for the values observed at ARE. For $T < 20$ s they are negative, indicating slower-than-expected group velocities, but for $20 \le T \le 80$ s, they are strongly positive, reaching a maximum of 0.094 km s^{-1} at $T \sim 30$ s. Such large residuals suggest that the group delays measured at ARE are not well modelled with only the first summation in eq. (2). The second summation must also be included to model an upper mantle velocity heterogeneity centred beneath the paths to ARE.

This unexpected conclusion is supported by the velocity residuals computed for the ANT and NNA measurements. Residuals for ANT are weakly positive ($\delta U < 0.05$ km s^{-1}) for $20 \le T \le 45$ s. They are zero for $T > 45$ s, indicating that the hypothesized heterogeneity does not extend very far south or very deep. The pattern of residuals for the NNA

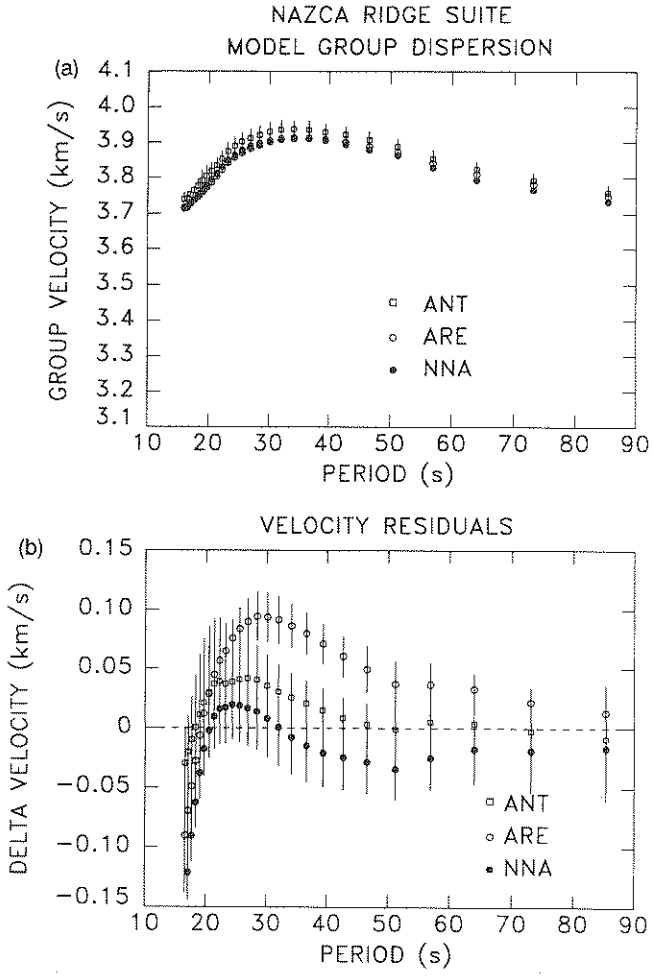

Figure 5. (a) Nazca ridge suite model dispersion curves calculated from age-dependent, anisotropic, pure-path values. Note that differences among the mean curves, averaged over the paths to each station, are less than 1 per cent. This agreement indicates that the large differences among the observed curves cannot be explained entirely by the effects of azimuthal anisotropy. Also note that the short-period velocities computed for NNA are faster than are observed. (b) Nazca ridge suite velocity residuals. Note, in particular, the negative residuals for NNA for $T \leq 20$ s, and the positive residuals for ANT for $T \geq 20$ s.

measurements is more complex, but consistent with the requirement of velocity heterogeneity in the upper mantle not directly related to the Nazca ridge structure. For $T < 20$ s the residuals are strongly negative, reflecting, presumably, the thick crust along the ridge's longitudinal axis. For $20 \leq T \leq 33$ s, the residuals are weakly positive (~ 0.02 km s^{-1}), in concert with the residuals at ANT. For $33 \leq T \leq 80$ s, the residuals are again slightly negative. Overall, the pattern of residuals indicates slow, poorly modelled short-period velocities along the Nazca ridge, and fast, poorly modelled intermediate-period group velocities in a previously unsuspected zone centred along the paths to ARE.

This data set is not adequate to localize the intermediate period (upper mantle) heterogeneity because all of the paths traverse the Nazca plate in the same direction; it

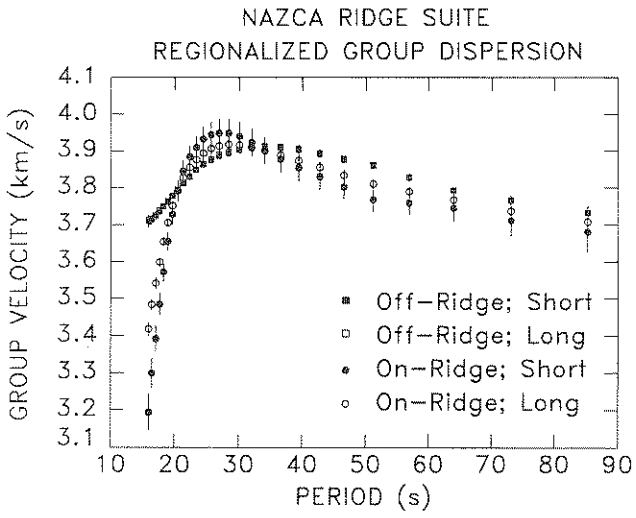

Figure 6. Nazca ridge suite dispersion curves, regionalized using eqs (1)–(5) to isolate the off-ridge and on-ridge group velocities. Assuming either a short or a long Nazca ridge yields the same off-ridge group velocities, but distinctly different on-ridge values. For both the short and long ridge cases the short-period group velocities are much slower than predicted.

contains no crossing paths. We can, however, compare the group velocity measurements with available tomographic images of the upper mantle. Our results are inconsistent with those of Nishimura & Forsyth (1988), which show a low velocity zone (~ -2 per cent) for periods of 33, 59, and 91 s off the central coast of South America. They are, however, consistent with the results of Zhang & Tanimoto (1989, 1991), and of Anderson, Tanimoto & Zhang (1992), which display a salient of faster ($\sim +1$ per cent) velocities at depths of 40–50 km, centred over the continental margin near ARE, and extending seaward to about 25°S, 85°W. The recognized Nazca ridge lies partly along the northwestern edge (average velocity) of this zone, which explains why the NNA data exhibit the smallest positive residuals in Fig. 5(b). Most importantly, it is clear that neither the ANT nor the ARE group velocities should be taken as representing typical lithosphere.

Figure 6 illustrates the dispersion curves constructed with eqs (1)–(5) and assigning the deviations from the NNA model curves to a short and a long Nazca ridge. Distributing the velocity residuals throughout the short, recognized edifice yields a sharply peaked dispersion curve with velocities varying from a minimum of 3.19 km s^{-1} at $T = 16$ s to a maximum of 3.95 km s^{-1} at $T = 28$ s. Distributing the velocity residuals throughout the longer, hypothetical edifice yields a curve that is less sharply peaked. It varies from 3.42 km s^{-1} at $T = 16$ s to 3.92 km s^{-1} at $T = 28$ s. Both curves exhibit group velocities that are slightly less than the model values at longer periods, but approach them at 90 s (Table 2).

Sala y Gomez suite

Isolating the group dispersion along the Sala y Gomez chain is made difficult because of the division of the measurements

Table 2. Age-dependent, anisotropic regionalized group velocities, Nazca ridge suite.

	Short Nazca Ridge				Long Nazca Ridge			
T (s)	*Off* (km s^{-1})	2-σ (km s^{-1})	*On* (km s^{-1})	2-σ (km s^{-1})	*Off* (km s^{-1})	2-σ (km s^{-1})	*On* (km s^{-1})	2-σ (km s^{-1})
16.0	3.710	0.018	3.194	0.048	3.714	0.012	3.418	0.018
16.5	3.714	0.014	3.299	0.040	3.716	0.010	3.483	0.016
17.1	3.725	0.012	3.392	0.034	3.727	0.008	3.542	0.014
17.7	3.737	0.010	3.484	0.030	3.739	0.008	3.599	0.012
18.3	3.750	0.008	3.572	0.026	3.751	0.008	3.654	0.012
19.0	3.763	0.008	3.655	0.026	3.764	0.008	3.705	0.012
19.7	3.778	0.008	3.728	0.028	3.779	0.008	3.751	0.012
20.5	3.795	0.008	3.791	0.028	3.796	0.008	3.791	0.012
21.3	3.812	0.008	3.844	0.030	3.813	0.008	3.827	0.014
22.3	3.830	0.008	3.884	0.030	3.831	0.008	3.855	0.014
23.3	3.849	0.008	3.909	0.032	3.850	0.008	3.876	0.016
24.4	3.863	0.008	3.932	0.034	3.865	0.010	3.894	0.016
25.6	3.876	0.010	3.944	0.036	3.878	0.010	3.906	0.016
26.9	3.887	0.010	3.949	0.036	3.890	0.010	3.914	0.018
28.4	3.895	0.010	3.949	0.038	3.898	0.010	3.918	0.018
30.1	3.903	0.010	3.940	0.038	3.905	0.010	3.916	0.018
32.0	3.908	0.010	3.923	0.038	3.911	0.010	3.910	0.018
34.1	3.911	0.010	3.901	0.038	3.914	0.010	3.900	0.016
36.6	3.910	0.010	3.878	0.036	3.912	0.010	3.888	0.016
39.4	3.904	0.010	3.854	0.036	3.906	0.010	3.873	0.016
42.7	3.892	0.010	3.830	0.034	3.894	0.010	3.855	0.014
46.5	3.877	0.010	3.802	0.032	3.879	0.008	3.834	0.014
51.2	3.861	0.010	3.768	0.032	3.863	0.008	3.810	0.014
56.9	3.828	0.010	3.759	0.032	3.829	0.008	3.790	0.014
64.0	3.794	0.010	3.745	0.036	3.794	0.010	3.767	0.016
73.1	3.766	0.012	3.711	0.042	3.766	0.012	3.737	0.020
85.3	3.734	0.016	3.681	0.054	3.733	0.016	3.708	0.026

into subgroups A and B. This division appears to be real. It is not caused by detectable errors in the revised epicentres; these were checked and verified. Thus, the immediate problem is to decide which of the groups, A or B, better samples the velocity structure along the Sala y Gomez chain. Group A consists of the four most northerly paths which may have been affected by the Easter fracture zone. Some of the paths in Group B, however, might have failed to sample the chain because of its narrow width.

To resolve this question, we computed the model dispersion curve for each path in the suite using eq. (4). These curves were then averaged in three ways: combining all model values, combining all values from Group A, and combining all values from Group B. Fig. 7(a) illustrates these mean curves, which are nearly identical. Based on the geometry of the propagation paths, no differences among the curves should be expected.

If the velocity residuals are computed, the patterns illustrated in Fig. 7(b) emerge. When all of the paths are included, the average residuals are about zero, except perhaps at the shortest periods. When the two subgroups of results are treated separately, Group A exhibits residuals of $\sim+0.05$ km s^{-1} for $T \geq 30$ s, whereas Group B exhibits slightly negative residuals for the entire period range. The negative residuals of Group B are what would be expected if the Sala y Gomez chain retards Rayleigh waves in the same way as the Nazca ridge.

Attributing Group A's positive residuals to the structure of the Sala y Gomez chain results in maximum group velocities along the chain of $\sim$4.03 km s^{-1} ($T \sim 35$ s), about 2 per cent *faster* than calculated for the path geometry. This value implies relatively fast upper mantle shear velocities in

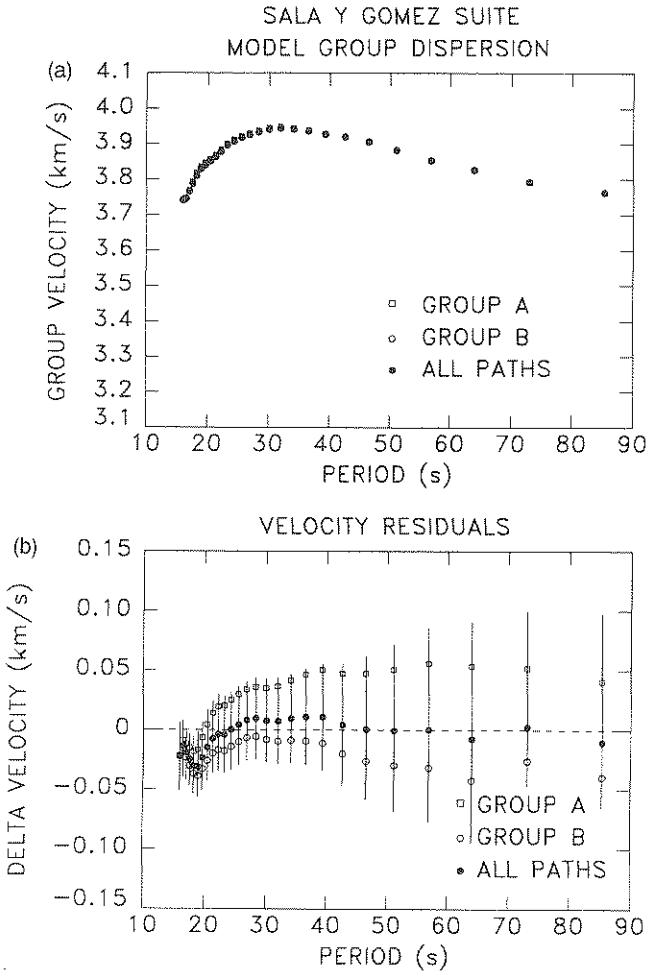

Figure 7. (a) Sala y Gomez suite model dispersion curves calculated from age-dependent, anisotropic pure-path values. Note that the curves illustrated here are averaged in three ways: over the total number of paths, over subgroup A and over subgroup B. Regardless of the averaging scheme, the curves are identical. (b) Sala y Gomez suite velocity residuals. Note that the residuals for the total suite average are nearly zero across the bandwidth. In contrast, the residuals for subgroup A are positive; those for subgroup B are weakly negative.

a relatively small area. More likely is that some other heterogeneity along the paths comprising Group A is responsible for the positive residuals.

Two possible locations for this hypothetical zone are the salient of fast, intermediate-period velocities observed adjacent to the coast of South America, and the fractions of the propagation paths north of the Easter fracture zone (~25°S). We reject the 'South American Salient' as the cause, for all paths in the suite intersect this area for about one-third of their total length. Attributing the residuals to the fractional path lengths north of the Easter fracture zone yields ambiguous results with eqs (1)–(5) because of the small data set. However, when the mean dispersion curve for Group A is graphed against the age-dependent group velocities, it matches nearly exactly the curve for oceanic lithosphere with age $\geq$ 20 Myr. This match suggests that the paths comprising Group A indeed sample a greater fraction of older lithosphere than we can determine

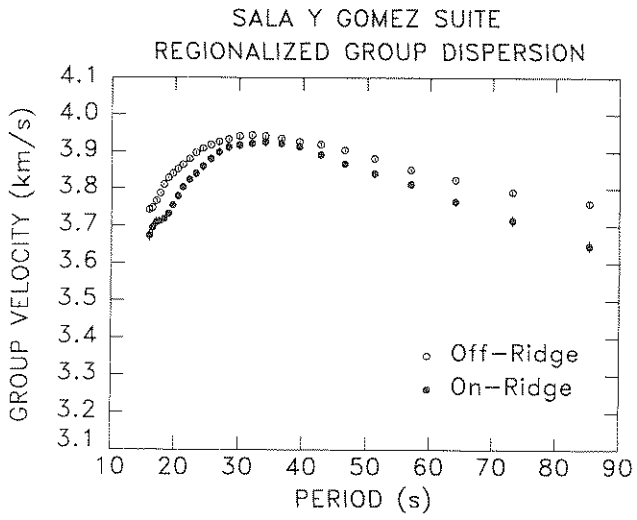

Figure 8. Sala y Gomez suite dispersion curves, regionalized using eqs (1)–(5) on subgroup B to isolate the off-ridge and on-ridge group velocities. The differences between these two curves are slight, being at most 3 per cent at $T = 80$ s. Note especially the on-ridge values for $T \leq 20$ s.

Table 3. Age-dependent, anisotropic regionalized group velocities, Sala y Gomez suite.

T (s)	*Off* (km s^{-1})	2-σ (km s^{-1})	*On* (km s^{-1})	2-σ (km s^{-1})
16.0	3.743	0.006	3.674	0.016
16.5	3.748	0.005	3.695	0.014
17.1	3.767	0.004	3.710	0.012
17.7	3.788	0.003	3.714	0.009
18.3	3.811	0.003	3.719	0.008
19.0	3.829	0.003	3.733	0.008
19.7	3.841	0.003	3.755	0.008
20.5	3.853	0.004	3.780	0.009
21.3	3.865	0.004	3.804	0.010
22.3	3.880	0.004	3.825	0.011
23.3	3.897	0.004	3.841	0.011
24.4	3.909	0.004	3.861	0.011
25.6	3.919	0.004	3.881	0.011
26.9	3.927	0.004	3.899	0.011
28.4	3.934	0.004	3.913	0.011
30.1	3.942	0.004	3.918	0.010
32.0	3.945	0.004	3.923	0.010
34.1	3.942	0.004	3.926	0.011
36.6	3.936	0.004	3.923	0.010
39.4	3.927	0.004	3.914	0.010
42.7	3.920	0.004	3.892	0.010
46.5	3.905	0.004	3.868	0.010
51.2	3.882	0.004	3.842	0.010
56.9	3.852	0.004	3.813	0.011
64.0	3.825	0.004	3.766	0.011
73.1	3.791	0.005	3.715	0.013
85.3	3.761	0.006	3.647	0.015

from the age map of Acton & Petronotis (1991). Given the grazing incidence of these four paths at the depth discontinuity of the fracture zone, it seems possible that they were deflected from the great circle, remained in the older lithosphere north of the fracture zone, and consequently did not sample the Sala y Gomez structure. We therefore discard the Group A measurements, and use only the Group B values to compute the velocity heterogeneity along the Sala y Gomez chain.

Figure 8 illustrates the group dispersion off and on the Sala y Gomez chain (Table 3), computed using the velocity measurements of Group B. Immediately apparent is that the on-ridge structure departs only slightly from the average, off-ridge structure. At $T = 83$ s, the on-ridge group velocity is about 3 per cent slower than the off-ridge value. For $T \leq 30$ s, the on-ridge structure is also slower, but only by at most 2.5 per cent. The small notch in the on-ridge dispersion curve at $T < 20$ s is probably not real. It results from the magnification of differences between the observed dispersion curves and the model curves, which exhibit a slight change in slope at these periods. Regardless, the short-period velocities are about 3.7 km s^{-1}, about 16 per cent faster than determined for the short Nazca ridge and about 9 per cent faster than determined for the hypothetical long Nazca ridge. In either case, it is clear that the Sala y Gomez chain does not slow Rayleigh wave propagation nearly as much as does the Nazca ridge.

INVERSION FOR MODELS OF V_{SV}

To determine the velocity structure along the Nazca ridge and Sala y Gomez chain, we inverted the on-ridge dispersion curves with a generalized least-squares program (Herrmann 1987). This program uses the algorithm of Rodi *et al.* (1975) to compute the partial derivatives of group velocity for inclusion in the data kernel, and accepts *a priori* information through a layer weighting scheme in which model velocities are allowed to vary more or less depending on available constraints. Following Russell (1987), we damped the differences between successive model layer velocities instead of individual values, thus constraining the gradient of the solution vector, rather than its magnitude. We thus obtained relatively smooth velocity models while allowing discontinuities to occur where demanded by the observations. Previous uses of this procedure (Woods, Russell & Herrmann 1989; Woods *et al.* 1991) have yielded reasonable results in continental and oceanic settings.

For these experiments, the modelling philosophy was to begin by discretizing the model space as a water layer over a stack of many flat, thin (e.g. 3 km) layers with uniform velocity. Such a parameterization approximates a half-space continuum, and represents the least biased starting model possible. After three or four iterations, groups of layers with generally similar velocity often became apparent, and these groups were sometimes separated by sharper discontinuities. Thus, the first inversions served as guides for the parameterization in subsequent inversions, where groups of layers were considered as thicker blocks. Following this procedure allowed us first, to explore the model space systematically, second, to find the depth of the crust–mantle interface with few preconceptions, and third, to construct

the simplest velocity models consistent with the observed dispersion.

Nazca ridge suite

The low short-period group velocities for both the short- and long-Nazca ridge cases suggest the presence of thick crust along the edifice. At short periods, however, the trade-off between the effects of ocean depth and crustal thickness warrant caution in this interpretation. We therefore conducted a series of inverse experiments with various parameterizations to ascertain the most likely values of crustal thickness for the two cases.

The next figures illustrate the modelling philosophy. Fig. 9(a) shows a model constructed for the short Nazca ridge using a single water layer ($h_1 = 3.75$ km), above 21 solid layers ($h_i = 3.0$ km). The dotted line represents the starting model, in which model layers 2 and 3 (ml2, ml3) were assigned average crustal velocities, and the remaining layers were assigned average upper mantle values. Only the water velocity was held fixed during inversion. We did not include a sediment layer, because the thickness of the sediment cover of the northern Nazca plate averages about 200 m (Hussong *et al.* 1976), far thinner than is resolvable with the current data. Seismic reflection profiles indicate that sediment does accumulate to about 500 m in pockets at the north-eastern tip of the ridge (Erlandson, Hussong & Campbell 1981), but these do not extend along the axis, and thus may be neglected. The solid line represents the final result, which is also listed in Table 4, along with the errors of the estimated velocities and the widths of the resolving kernels.

Most important to the present study are the model results at shallow depth. First, a sharp discontinuity appears at about 10 km below mean sea-level. Above this discontinuity the velocities in ml2 and ml3 decreased from 3.9 to about 3.6 km s^{-1}. Below the discontinuity to a depth of about 25 km, the velocities decreased as a group, from 4.5 km s^{-1} (mantle values) to ~4.1 km s^{-1} (crustal values). It is therefore tempting to interpret the velocity grouping above the discontinuity as greatly thickened 'Layer 2' of the oceanic crust, and the grouping below the discontinuity as 'Layer 3'. Although these layers are useful idealizations, recent interpretations of marine refraction data (e.g. Lewis 1978; Spudich & Orcut 1980) show that *Vp* and *Vs* in Layer 2 increase linearly with depth; in Layer 3 they achieve some uniformity, although there remains variation. Thus, the interpretation of a thick Layer 2 is not strictly justified. The accompanying resolving kernels illustrate, moreover, that the values in ml2 and ml3 above the discontinuity are not well resolved. All that may be concluded is that V_{SV} is low. Regardless, it is clear that if we require that the velocity contributions from lateral heterogeneity be restricted to the short, recognized Nazca ridge, then we must conclude that the crust along the ridge is about 18–21 km thick.

In the upper mantle, the model shows the development of

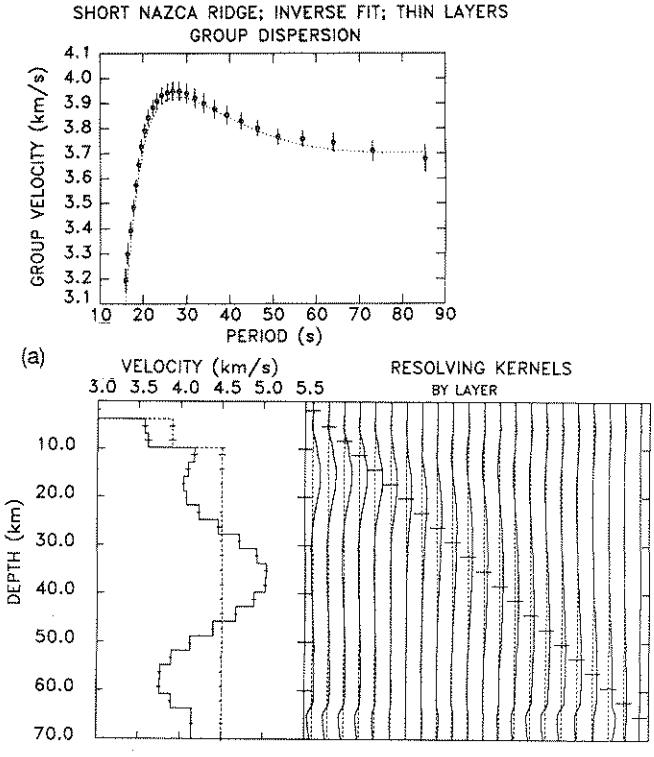

Figure 9(a). Summary of finely layered inverse model for short Nazca ridge. Top: filled circles represent on-ridge group velocities; error bars represent two standard deviations; dashed line is inverse fit to observations. Bottom: on left, dashed line represents starting model of V_{SV}; solid line represents final result. On right, resolving kernels normalized to maximum value.

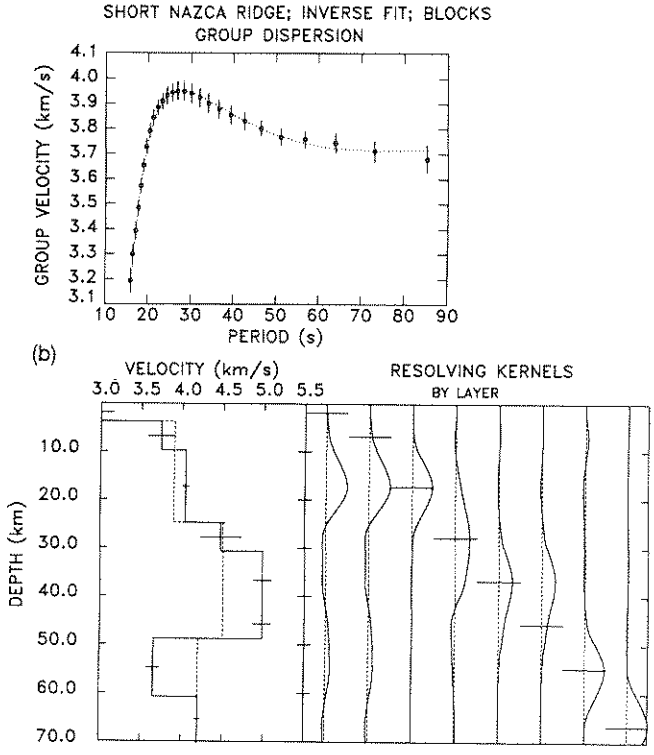

Figure 9(b). Summary of simplified inverse model for short Nazca ridge. Top: filled circles represent on-ridge group velocities; error bars represent two standard deviations; dashed line is inverse fit to observations. Bottom: on left, dashed line represents starting model of V_{SV}; solid line represents final result. On right, resolving kernels normalized to maximum value.

Table 4. Inverse models for V_{SV}, short Nazca ridge.

layer ml_i	h_i (km)	V_{SV}^{start} (km s^{-1})	V_{SV}^{final} (km s^{-1})	σ (km s^{-1})	w_k (km)
		Detailed Parameterization			
1	3.75	0.00	0.00	0.04	36
2	3.00	3.90	3.58	0.04	36
3	3.00	3.90	3.61	0.04	34
4	3.00	4.50	4.17	0.04	30
5	3.00	4.50	4.09	0.03	23
6	3.00	4.50	4.04	0.01	14
7	3.00	4.50	4.07	0.01	10
8	3.00	4.50	4.23	0.02	16
9	3.00	4.50	4.46	0.02	20
10	3.00	4.50	4.72	0.02	20
11	3.00	4.50	4.92	0.02	19
12	3.00	4.50	5.03	0.02	18
13	3.00	4.50	5.02	0.02	22
14	3.00	4.50	4.89	0.02	26
15	3.00	4.50	4.67	0.02	27
16	3.00	4.50	4.39	0.01	26
17	3.00	4.50	4.12	0.01	25
18	3.00	4.50	3.89	0.02	25
19	3.00	4.50	3.76	0.02	24
20	3.00	4.50	3.76	0.02	22
21	3.00	4.50	3.89	0.02	11
22	---	4.50	4.15	0.02	---
		Simplified Parameterization			
1	3.75	0.00	0.00	0.16	21
2	6.00	3.90	3.74	0.16	21
3	15.00	3.90	4.04	0.04	15
4	6.00	4.50	4.48	0.25	14
5	12.00	4.50	4.98	0.11	12
6	6.00	4.50	4.98	0.11	10
7	12.00	4.20	3.66	0.06	15
8	---	4.20	4.20	0.03	---

a high-velocity lid. Note that at $z \sim 38$ km V_{SV} increased from 4.5 km s^{-1} to about 5.0 km s^{-1} to fit the group velocities ($25 \leq T \leq 35$ s) that generate the positive residuals in Fig. 5(b). We estimate that the lid is about 27 km thick. The model also displays a strongly developed low-velocity zone (LVZ), in which V_{SV} decreases to about 3.8 km s^{-1}.

The resolving kernels generally indicate, however, that the shear velocities of the relatively thin layers used in this parameterization are not well resolved. Each of the kernels is low amplitude and spans a range of depths wider than a single layer thickness. This is especially true for $z > 30$ km. Note, however, that the kernel for ml6, in the centre of the lower crust, spans $10 \leq z \leq 25$ km, the depth range between the upper crustal discontinuity and the crust–mantle interface. Reparameterizing the crust to reflect this limitation should result in a viable model. Note also that the error bars on the layer velocities are underestimates, because the final damping values were not relaxed to zero. This was done to prevent small eigenvalues from contaminating the solution.

Figure 9(b) shows a reparameterization of the model space into thicker blocks as guided by the results in the first inversion (Table 4). Here, we have kept the ocean depth fixed, and have assigned crustal velocities (3.9 km s^{-1}) to the next two layers, which have thicknesses of 6 and 15 km. The high-velocity lid was assigned a typical upper mantle velocity (4.5 km s^{-1}), and was divided into three layers of 6, 15, and 6 km. Below, the mantle low-velocity zone (LVZ) was assigned a value of 4.2 km s^{-1}.

Upon inversion, the velocity model changed little at shallow depths. V_{SV} in the hypothetical, thick crustal sequence increased only to 4.04 km s^{-1}, remaining in the range for values within the lower crust. It is important to note that ml3 controls the fit to the observations at short periods. There is no resolution of the ocean layer or of the 6 km upper crust. The resolving kernels for these layers are both centred on ml3. Moreover, ml3 appears to be well resolved; its kernel is large amplitude (~0.93) and spans its depth range. Although this image is not perfectly resolved, it again seems clear that if the lateral heterogeneity required to explain the observations is assigned to the short Nazca ridge, then the ridge must be about 20 km thick.

The largest changes in the inverse model occurred in the lid and LVZ. In the lid, ml5 and ml6 increased by ~10 per cent to 5.0 km s^{-1}, reflecting the 'South American Salient' discussed above. The upper two layers of the lid (ml4 and ml5) are fairly well resolved, but V_{SV} in ml6 appears to depend strongly on information from ml5. Shear velocity in the LVZ decreased ~13 per cent to 3.7 km s^{-1}; this value is also fairly well resolved. It is important to realize, however, that the strong velocity contrast between the lid and the LVZ (~30 per cent) is forced upon the model by the requirement that the velocity heterogeneity at all periods be explained by the Nazca ridge.

We next examine the hypothesis that the Nazca ridge actually extends to the extinct Roggeveen rise by inverting the on-ridge group dispersion curve constructed for the long Nazca ridge. Here we follow the same procedure in the inversion experiments: first parameterizing the model space as many thin layers, then simplifying the parameterization to optimize the resolution.

Because in this regionalization the heterogeneity is distributed over a larger area, the on-ridge dispersion curve is not so sharply peaked. As a consequence, the trial velocity model, shown as the solid line in Fig. 10(a), does not exhibit the extreme values as did the trial model for the short ridge. Again, the dotted line shows the starting model (Table 5). In this case we used a slightly thinner water layer ($h_1 = 3.0$ km) to reflect the average ocean depth along the hypothetically longer ridge structure. In the crust $V_{SV} = 3.9$ km s^{-1}, and in the mantle V_{SV} was a uniform 4.5 km s^{-1}. Upon inversion, V_{SV} in ml2 and ml3 decreased to about 3.5 km s^{-1}, and in ml4, ml5, and ml6 it decreased to about 4.0 km s^{-1}. Thus it appears that the crust is about 15 km thick, although ml7 might be included for a total thickness of 18 km. Below, V_{SV} increases gradually to form the mantle lid, with maximum values of about 4.7 km s^{-1}. The mantle LVZ then appears, where V_{SV} decreases to

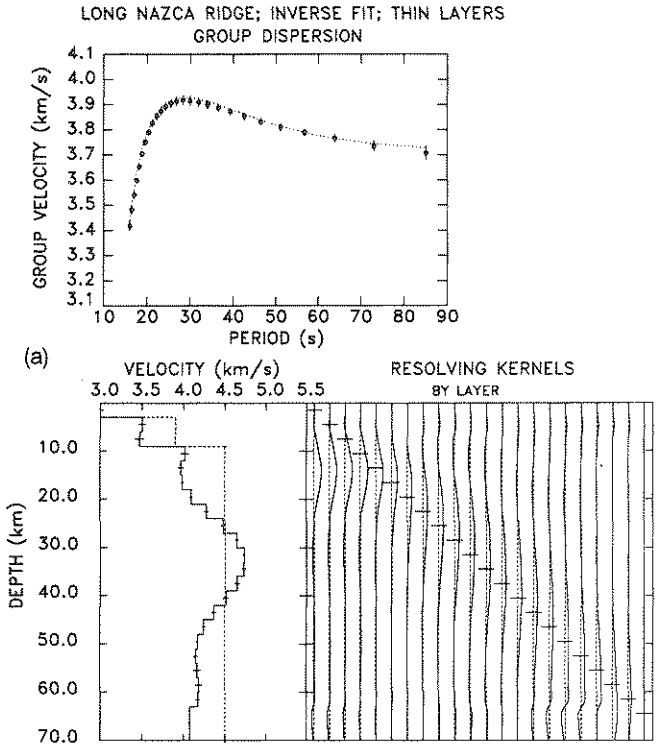

Figure 10(a). Summary of finely layered inverse model for long Nazca ridge. Top: filled circles represent on-ridge group velocities; error bars represent two standard deviations; dashed line is inverse fit to observations. Bottom: on left, dashed line represents starting model of V_{SV}; solid line represents final result. On right, resolving kernels normalized to maximum value.

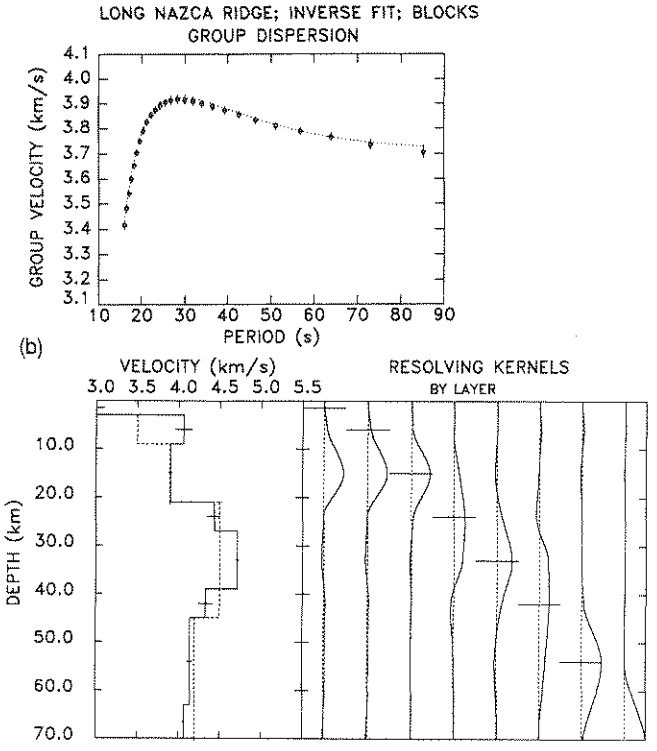

Figure 10(b). Summary of simplified inverse model for long Nazca ridge. Top: filled circles represent on-ridge group velocities; error bars represent two standard deviations; dashed line is inverse fit to observations. Bottom: on left, dashed line represents starting model of V_{SV}; solid line represents final result. On right, resolving kernels normalized to maximum value.

about $4.0\,\mathrm{km\,s^{-1}}$. Note again that with the model parameterization being thin layers, the errors are underestimated. Moreover, the resolution is poor, the best being achieved in the lower crust (ml5 and ml6).

By reparameterizing the model space as thicker blocks, the model illustrated in Fig. 10(b) was obtained. We consider this model to be the best of the four presented, because it balances fit to the observed dispersion curve, simplicity, and resolution. It also departs least from the starting model (Table 5). Only in ml2, the shallow crustal layer, does the final V_{SV} differ more than 5 per cent from its starting value. This large adjustment reflects the lack of resolution for $z \leq 10\,\mathrm{km}$. Once again the lower crust controls the fit to the observations for $T \leq 20\,\mathrm{s}$. The lid and the LVZ are also relatively well resolved. V_{SV} in the lid is probably underestimated, however, because the on-ridge group velocities in the period range $20 \leq T \leq 50\,\mathrm{s}$ are affected by the 'South American Salient', which does not extend as far westward as the long Nazca ridge. In other words, attributing the fastest group velocities to the long ridge smears the heterogeneity over a larger space than it actually covers. Nevertheless, inverse models constructed with the assumption of a long Nazca ridge yield an average crustal thickness of 15–18 km.

Sala y Gomez suite

As stated earlier, the average on-ridge dispersion curve for the Sala y Gomez Chain departs only slightly from the model dispersion curve. Thus, it appears that little is anomalous about Rayleigh wave propagation along this structure, a conclusion substantiated by the following two velocity models.

Figure 11(a) illustrates a trial model constructed with equal-thickness layers. In this case the layers were relatively thick, 15 km, because there are few details in the dispersion curve to understand. The most difficult choice in constructing this model was the selection of the ocean depth. To reiterate, bathymetry along the structure is rugged. Although individual seamounts comprising the chain often stand high above their surroundings (500–1000 m), they are small in area, so the mean ocean depth is not accurately represented by the value over the seamounts. Using that value in the starting model would result in artificially low crustal V_{SV} or in thick crust because of the trade-off between the effects of ocean depth and crust. Therefore, we averaged the DBDB5 values in the rectangular region defined by 25°S, 27°S, 105°W and 85°W, to determine a mean ocean depth of 3.5 km. The starting velocities were as in the Nazca ridge inversions: $3.9\,\mathrm{km\,s^{-1}}$ in the crust and $4.5\,\mathrm{km\,s^{-1}}$ in the uniform mantle (see Table 6 for model parameters).

As seen in the illustration, a reasonably good fit to the observed dispersion curve was achieved with this model, and it remained relatively simple. Beneath the water layer is a 6 km thick crust with normal values of $V_{SV} \sim 3.8\,\mathrm{km\,s^{-1}}$. Beneath the crust, the mantle velocity is also typical, $\sim 4.45\,\mathrm{km\,s^{-1}}$. These values are only about 2 per cent slower

Table 5. Inverse models for V_{SV}, long Nazca ridge.

layer ml_i	h_i (km)	V_{SV}^{start} (km s^{-1})	V_{SV}^{final} (km s^{-1})	σ (km s^{-1})	w_k (km)
		Detailed Parameterization			
1	3.00	0.00	0.00	0.04	24
2	3.00	3.90	3.50	0.04	24
3	3.00	3.90	3.48	0.05	20
4	3.00	4.50	4.02	0.05	16
5	3.00	4.50	3.97	0.03	13
6	3.00	4.50	3.99	0.01	12
7	3.00	4.50	4.10	0.01	12
8	3.00	4.50	4.28	0.03	13
9	3.00	4.50	4.48	0.03	15
10	3.00	4.50	4.65	0.02	18
11	3.00	4.50	4.74	0.01	20
12	3.00	4.50	4.73	0.02	20
13	3.00	4.50	4.65	0.03	17
14	3.00	4.50	4.51	0.03	17
15	3.00	4.50	4.37	0.03	22
16	3.00	4.50	4.24	0.02	24
17	3.00	4.50	4.17	0.01	23
18	3.00	4.50	4.15	0.03	21
19	3.00	4.50	4.17	0.04	20
20	3.00	4.50	4.19	0.04	20
21	3.00	4.50	4.17	0.03	12
22	---	4.50	4.07	0.01	---
		Simplified Parameterization			
1	3.00	0.00	0.00	0.00	12
2	6.00	3.50	4.06	0.10	12
3	12.00	3.90	3.90	0.02	12
4	6.00	4.50	4.44	0.09	14
5	12.00	4.50	4.72	0.02	12
6	6.00	4.50	4.33	0.09	18
7	18.00	4.20	4.14	0.03	18
9	---	4.20	4.07	0.01	---

than the starting values. Unlike the observations along the Nazca ridge, the observations along the Sala y Gomez chain do not require an anomalously thick crust. Deeper in the mantle, V_{SV} decreases to a minimum of 3.9 km s^{-1} at $z = 75$ km. One curious aspect of the model is the apparent secondary low-velocity zone centred at $z \sim 33$ km. This feature emerged as damping was relaxed in this inversion, and in other trials using fine layering. Such a reversal seems implausible, and probably results from poor resolution at these depths. As seen in the resolving kernels for ml4 and ml5, the estimates for V_{SV} in these layers depend to a large degree on information from the layers immediately above and below them. The best resolved layer is ml3, the lid cap, where the kernel spans ml3 and only about one-half of ml4. Note that neither the water layer, ml1, nor the crust, ml2, are really well resolved, however.

Attempts to optimize the resolution matrix by re-parameterizing the model space met little success. Fig. 11(b) (and Table 6b) shows one such attempt, in which ml3, ml4, and ml5 of the previous inversion were considered as a single block, 45 km thick. As expected, this resulted in a slightly worse fit to the observed dispersion curve because there were two fewer adjustable parameters. Not expected, however, was that the degraded fit occurred at the short-period end of the curve. This degradation and the resolving kernel for ml2, which spans the depth range for ml3, $10 \leq z \leq 54$ km, suggest that the Sala y Gomez group velocities cannot resolve the shallow velocity structure. Nevertheless, the deeper structure is well resolved, and it appears to be typical. In neither of the Sala y Gomez inversions did the upper mantle appear to be anomalously slow.

DISCUSSION

The investigations reported above have established that the dispersion of short-period Rayleigh waves in the vicinity of the Nazca ridge requires lateral velocity heterogeneity. If this heterogeneity is attributed to the recognized, 1200 km long edifice, the crust along the ridge must be about 20 km thick. If, however, the heterogeneity is attributed to the longer, 2200 km edifice hypothesized in this paper, the crust is 15–18 km thick. In contrast, there does not appear to be appreciable heterogeneity along the Sala y Gomez chain; the crust along this structure is of normal thickness. These estimates of crustal thickness, h_c, substantiate values derived earlier from sonobuoy data (Principal 1974; Cutler 1977).

Our estimates of h_c also compare favourably with estimates made from isostatic balance calculations. Haxby's (1987) map of oceanic free-air gravity anomalies shows that over the Nazca ridge, and over its hypothetical extension, $\delta g_{FA} \leq 10$ mgal. Thus, this structure appears to be nearly in isostatic equilibrium. Over some of the small seamounts of the Sala y Gomez chain, δg_{FA} is as large as 30 mgal, which indicates that they are not completely compensated. Nevertheless, the broader region of shallow residual bathymetry on which the chain sits (250 m isobath; Fig. 1b) exhibits $\delta g_{FA} \leq 10$ mgal, so it is nearly in equilibrium. If we assume equilibrium for the average structures, and representative values for the crust and upper mantle ($h_c = 6$ km, $\rho_c = 3000$ kg m^{-3}, and $\rho_m = 3300$ kg m^{-3}), then we obtain the following. Along the Sala y Gomez chain, $h_c = 8$ km. Along the recognized Nazca ridge, $h_c = 18$ km, but along its hypothetical extension, $h_c = 12$ km. If the last two values are averaged, $h_c = 15$ km, in agreement with the lower estimate from surface waves along the extended ridge, and with the value derived independently by Couch & Whitsett (1981) from free-air gravity.

The values of h_c along the Nazca ridge may also be compared with those on its mirror image on the Pacific plate, the Tuamotu plateau. There, Talandier & Okal (1987) determined that $22 \leq h_c \leq 27$ km (their Models 2, 3 and 4). Local measurements of phase velocity beneath Rangiroa Atoll on the western side of the plateau suggested $h_c \sim 35$ km, but the atoll is not representative of the whole structure. Thus, the larger values of h_c for the Nazca ridge agree with the smaller values (their Model 2) for the

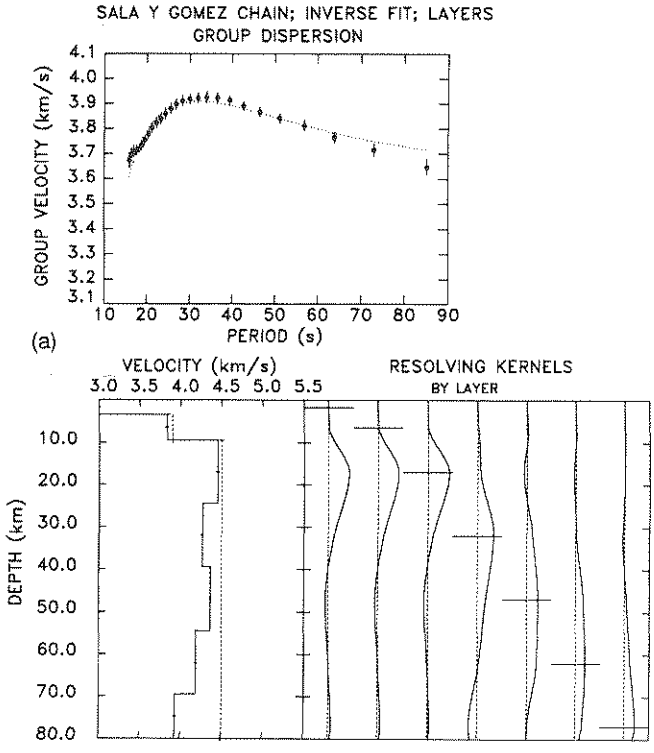

Figure 11(a). Summary of layered inverse model for Sala y Gomez chain. Top: filled circles represent on-ridge group velocities; error bars represent two standard deviations; dashed line is inverse fit to observations. Bottom: on left, dashed line represents starting model of V_{SV}; solid line represents final result. On right, resolving kernels normalized to maximum value.

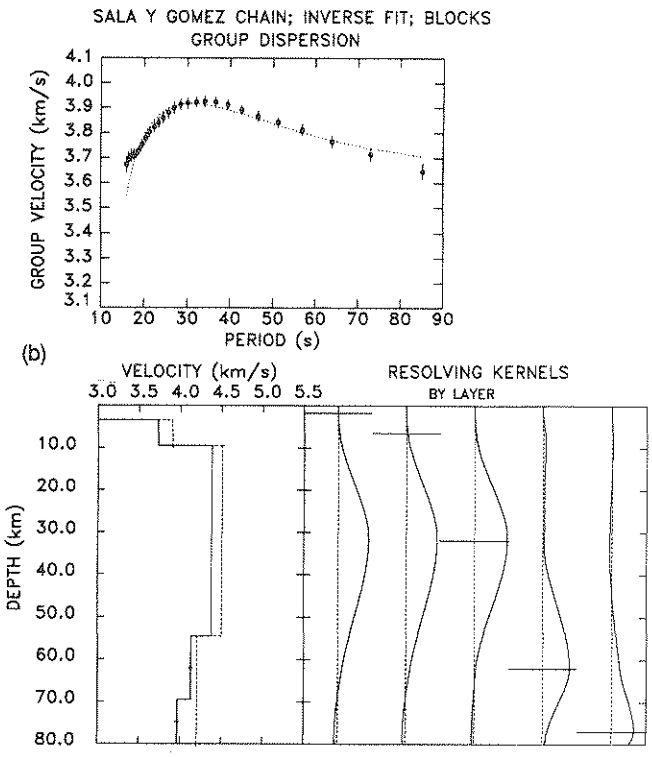

Figure 11(b). Summary of simplified inverse model for Sala y Gomez chain. Top: filled circles represent on-ridge group velocities; error bars represent two standard deviations; dashed line is inverse fit to observations. Bottom: on left, dashed line represents starting model of V_{SV}; solid line represents final result. On right, resolving kernels normalized to maximum value.

Table 6. Inverse models for V_{SV}, Sala y Gomez chain.

layer ml_i	h_i (km)	V_{SV}^{start} (km s^{-1})	V_{SV}^{final} (km s^{-1})	σ (km s^{-1})	w_k (km)
		Detailed Parameterization			
1	3.50	0.00	0.00	0.00	19
2	6.00	3.90	3.83	0.02	19
3	15.00	4.50	4.45	0.02	19
4	15.00	4.50	4.27	0.02	34
5	15.00	4.50	4.37	0.01	25
6	15.00	4.50	4.19	0.02	27
7	---	4.50	3.93	0.02	---
		Simplified Parameterization			
1	3.50	0.0	0.00	0.01	12
2	6.00	3.90	3.73	0.01	12
3	45.00	4.50	4.38	0.01	45
4	15.00	4.20	4.13	0.02	15
5	---	4.20	3.96	0.03	---

Tuamoto plateau to within ~20 per cent. Given the uncertainties of the single-station measurements and the resolution of the inverse models reported here, it is reasonable to conclude that the crust along the Nazca ridge and that along the Tuamotu plateau are of about the same thickness. This conclusion, coupled with the apparent correspondence in age progression along each of the two structures, strengthens the idea that they shared a common origin. We note, however, that the differences in their sizes, and hence volumes, implies an asymmetry in their production rates.

Also remaining unclear is how the Nazca ridge and Sala y Gomez chain fit into the kinematic evolution of the Farallon–Nazca–Pacific plate system. One scenario for this evolution begins with the observation that the Nazca ridge intersects the Sala y Gomez chain at an oblique angle (~130°) near the middle of the Nazca plate, thus appearing to be continuous with that structure. This spatial relationship led Morgan (1972) to suggest that the two structures formed as the Farallon (later Nazca) plate first moved north-east, then east relative to a hotspot astride the Farallon–Pacific spreading centre. The change in strike of the structures would be analogous to (but not coeval with) the bend in the Hawaiian–Emperor seamount chain in the north-central Pacific. Based on ages of magnetic lineations (Cande *et al.* 1989) the change in plate velocity occurred

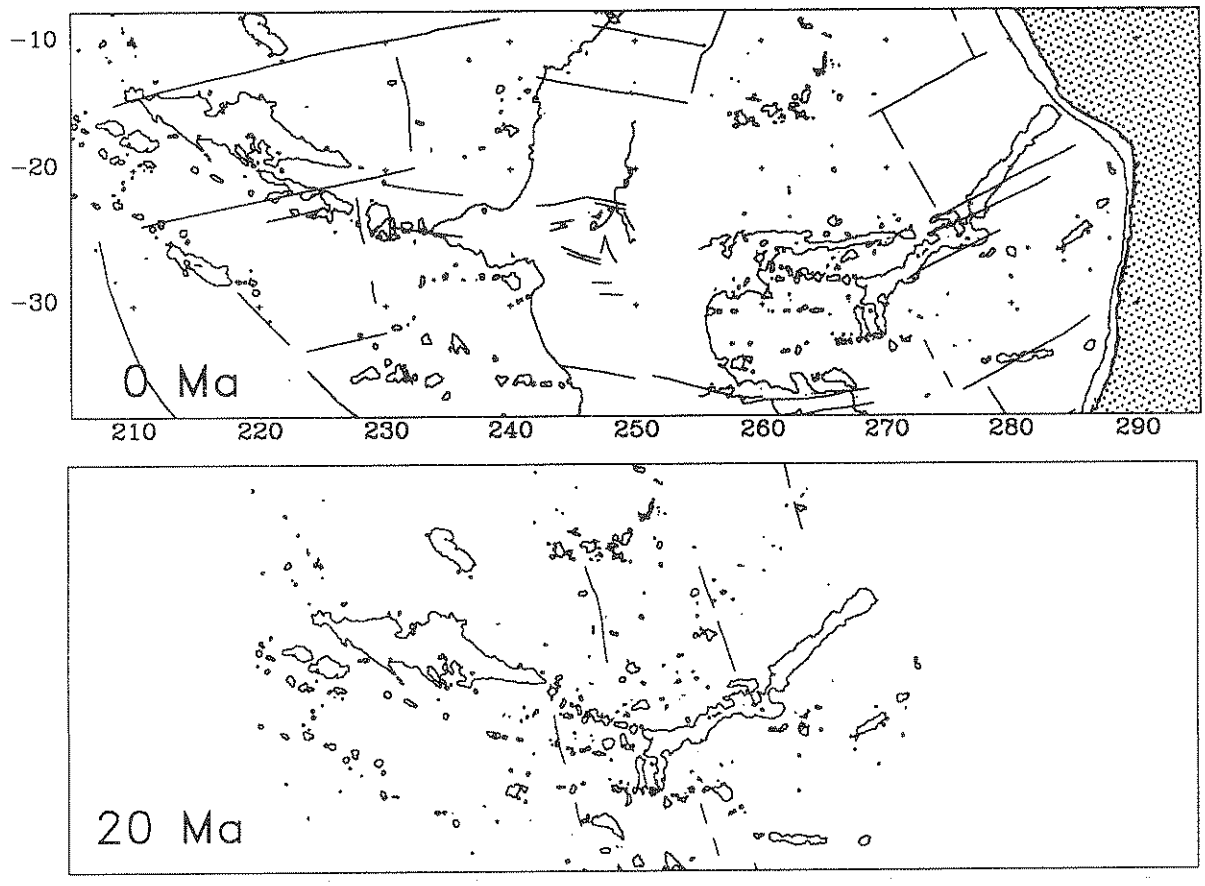

Figure 12. Preliminary reconstruction of extended Nazca ridge and Tuamotu plateau. Top: current configuration of Nazca–Pacific spreading centre, aseismic ridge edifices, and fracture zones. Magnetic anomaly 7 (26 Ma) illustrated for reference. Bottom: configuration at Chron 6 (20 Ma) obtained by rotating Nazca plate and Pacific plate about total reconstruction pole from Pilger & Handschumacher (1981). Note the alignment of the northern arm of the Tuamotu plateau with the extended Nazca ridge.

between Chron 10 (30 Ma) and Chron 7 (26 Ma). Therefore, by 26 Ma, the Nazca ridge and Tuamotu plateau had separated, and the Sala y Gomez chain began to form.

Although appealing in its simplicity, this model is inconsistent with several observations. Nearly all authors note that the Sala y Gomez chain is morphologically dissimilar to either the Nazca ridge or the Tuamotu plateau. As discussed earlier, it consists of small, irregularly shaped, disconnected seamounts, whereas the other structures are massive, coherent edifices. We have shown here that surface-wave dispersion measured along the axis of Sala y Gomez reveals no evidence of thickened oceanic crust, so it cannot be nearly so massive as the other structures. Finally, the few radiometric age dates for rocks along the chain (Baker, Buckley & Holland 1974; Clark & Dymond 1977; Bonatti *et al.* 1977) do not show a clear progression of ages from east to west. Taken together, these lines of evidence suggest that the Sala y Gomez chain is not a simple hotspot track.

Another, though weaker, argument against the Sala y Gomez chain being a hotspot track is the apparent discrepancy between the times of the changes in the Farallon–Pacific relative plate velocities and the Farallon–Pacific-hotspot velocities. In Morgan's model the Farallon-hotspot motion changed from north-east to east at about Chron 7 (26 Ma). However, the presence of the Mendoza–Roggeveen rise in the middle of the Nazca plate indicates that the locus of active spreading between the Pacific and Farallon plates remained stable until about Chron 6 (20 Ma), after which it jumped to its current position on the East Pacific rise (e.g. Herron 1972; Mammerickx *et al.* 1980). Although changes in relative plate velocities need not coincide with changes in absolute plate velocities, it seems likely that they would.

If the Nazca ridge is extended to the Roggeveen rise, as is proposed here, some of the geometric and kinematic difficulties in the evolution of the plate system noted by Pilger & Handschumacher (1981) are resolved. A detailed scenario for the kinematic evolution is beyond the scope of this paper, but a simple check of the concept is possible. Using Pilger & Handschumacher's total reconstruction poles we rotated the Nazca and Pacific plates into their configuration at Chron 6 (20 Ma). As seen in Fig. 12, the previously unrecognized seamount chain that extends west–north-west from the Roggeveen rise aligns with the northern arm of the Tuamotu plateau (Tatakoto, Pukaruha and Reao). The seamounts have not been dated, but the alignment suggests that they comprise the old, Pacific side mirror image of the extended Nazca ridge, and were formed by the Nazca hotspot on the Roggeveen rise. Moreover, they exhibit $\delta g_{FA} \leq 10$ mgal, indicating isostatic equilibrium and a likely origin at the spreading centre. Thus, the portion of the Nazca plate on which the seamounts reside is

probably old Pacific lithosphere which was added to the Nazca plate during the reorganization of the spreading centre. A key question is whether the seamounts are coeval with the surrounding sea-floor; future investigations should address this problem.

It seems clear, however, that the velocity of the Farallon plate relative to the Nazca hotspot remained largely unchanged until ~20 Ma when the Mendoza–Roggeveen rise was abandoned. Formation of the Nazca–Tuamotu edifice was interrupted only briefly as the hotspot volcanism moved from the Mendoza rise to the Roggeveen rise south of the Nazca fracture zone. In addition, the velocity of the Pacific plate relative to the Nazca hotspot appears to have remained fairly constant until this time. Thereafter, the complex reorganization of the Farallon–Pacific spreading centre began, which likely involved progressive ridge jumps and the formation and abandonment of various microplates.

In this scenario, the Sala y Gomez chain does not track the Farallon plate over the Nazca hotspot. Considering that the chain sits on the edge of a depth discontinuity (Fig. 2) similar to what is expected at large fracture zones, perhaps it represents a leaky transform fault. Handschumacher (1976) and Pilger & Handschumacher (1981) favoured this explanation, claiming that the chain formed in response to fractures propagating through the plate as its margins changed, an idea resurrected from Betz & Hess' (1942) work on the Hawaiian Swell.

CONCLUSION

In this paper, we have presented single-station measurements of Rayleigh wave group velocity made along two aseismic ridges in the eastern Pacific Ocean basin: the Nazca ridge and the Sala y Gomez chain. Using the pure-path technique to model the age dependence and anisotropy of the velocities along the propagation paths, we isolated the dispersion along each of the target structures. These dispersion curves, and the shear velocity models derived from them, substantiate earlier, tentative conclusions that the crustal thickness along the Nazca ridge is about 18 ± 3 km, but is only about 6 km along the Sala y Gomez chain. These values were shown to be consistent with values derived from free-air gravity anomalies.

An important result from this investigation is the recognition that the Nazca ridge does not terminate at its intersection with the Sala y Gomez chain, but extends another 1000 km south-west to the extinct Roggeveen rise. Extending north-west from the relict spreading centre is a small chain of seamounts that parallels the Tuamotu plateau. It therefore appears that the proposed extended Nazca ridge has a mirror image west of the Roggeveen rise. This scenario is compatible with the abandonment of the Mendoza–Roggeveen spreading centre at Chron 6 (20 Ma), but is inconsistent with the Sala y Gomez chain tracking the hotspot. The Sala y Gomez chain more likely represents a leaky transform fault. A detailed kinematic description of this evolution remains to be established, and may require the acquisition of more detailed magnetic and bathymetric data for the central Nazca plate.

ACKNOWLEDGMENTS

We thank Bob Herrmann and Dave Russell for the use of their surface-wave package, and many discussions about its uses and abuses. Clyde Nishimura answered our many questions about the pure-path technique. This research was supported in part by the Office of Naval Research and the National Science Foundation (grant EAR-9105-954).

REFERENCES

Acton, G. & Petronotis, K., 1991. Pacific marine magnetic lineations and the age of the seafloor, in *Data Synthesis on Rejuvenescent Mid-plate Volcanism in the Pacific Basin,* Vol. IV, pp. A.1–A.26, eds Gordon, R. & Shoberg, T., Joint Oceanographic Institutions, Washington, DC.

Anderson, D., Tanimoto, T. & Zhang, Y.-S., 1992. Plate tectonics and hotspots: the third dimension, *Science,* **256,** 1645–1651.

Baker, P.E., Buckley, F. & Holland, J.G., 1974. Petrology and geochemistry of Easter Island, *Contr. Mineral. Petrol.,* **44,** 85–100.

Båth, M., 1960. Crustal structure of Iceland, *J. geophys. Res.,* **65,** 1793–1807.

Betz, F. & Hess, H.H., 1942. The floor of the north Pacific Ocean, *Geog. Rev.,* **32,** 99–116.

Bonatti, E., Harrison, C.G.A., Fisher, D.E., Honnorez, J., Schilling, J.-G., Stipp, J.J., & Zentilli, M., 1977. Easter volcanic chain (southeast Pacific): a mantle hot line, *J. geophys. Res.,* **82,** 2457–2478.

Bott, M.H.P. & Gunnarsson, K., 1980. Crustal structure of the Iceland–Faeroe ridge, *J. Geophys.,* **47,** 221–227.

Cande, S.C., LaBrecque, J.L., Larson, R.L., Pitman, W.C., III, Golovchenko, X. & Haxby, W.E., 1989. Magnetic lineations of the world's ocean basins, in *AAPG Map,* AAPG, Tulsa.

Clark, J.G. & Dymond, J., 1977. Geochronology and petrochemistry of Easter and Sala Y Gomez Islands: implications for the origin of the Sala Y Gomez Ridge, *J. Volc. Geotherm. Res.,* **2,** 29–48.

Couch, R. & Whitsett, R.M., 1981. Structures of the Nazca Ridge and the continental shelf and slope of southern Peru, in *Nazca Plate: Crustal Formation and Andean Convergence, Geol. Soc. Am. Mem. 154,* pp. 569–586, eds Kulm, L.D., Dymond, J., Dasch, E.J. & Hussong, D.M., Geol. Soc. Am., Boulder, CO.

Cutler, S.T., 1977. Geophysical investigation of the Nazca Ridge, *MSc thesis,* University of Hawaii, Honolulu, Hawaii.

DeMets, C., Gordon, R.G., Argus, D.F. & Stein, S., 1990. Current plate motions, *Geophys. J. Int.,* **101,** 425–478.

Dziewonski, A.M. & Hales, A.L., 1972. Numerical analysis of dispersed seismic waves, in *Seismology: Surface Waves and Earth Oscillations, Methods in Computational Physics 11,* pp. 39–85, ed. Bolt, B., Academic Press, New York.

Engeln, J.F. & Stein, S., 1984. Tectonics of the Easter plate, *Earth planet. Sci. Lett.,* **68,** 259–270.

Erlandson, D.L., Hussong, D.M. & Campbell, J.F., 1981. Sediment and associated structure of the northern Nazca plate, in *Nazca Plate: Crustal Formation and Andean Convergence, Geol. Soc. Am. Mem.* 154, pp. 295–314, eds Kulm, L.D., Dymond, J., Dasch, E.J. & Hussong, D.M., Geol. Soc. Am., Boulder, CO.

Forsyth, D.W., 1975. The early structural evolution and anisotropy of the oceanic upper mantle, *Geophys. J.R. astr. Soc.,* **43,** 103–162.

Handschumacher, D.W., 1976. Post-Eocene plate tectonics of the eastern Pacific, in *The Geophysics of the Pacific Ocean Basin and its Margin* Geophys. Monogr. Ser., **19,** pp. 117–202, eds Sutton, G., Manghnani, M. & Moberly, R., Am. geophys. Un., Washington, DC.

Haxby, W.F, 1987. *Gravity Field of the World's Oceans*, NOAA, Boulder, Colorado.

Herrin, E. & Goforth, T., 1977. Phase-matched filters: application to the study of Rayleigh waves, *Bull. seism. Soc. Am.*, **67**, 1259–1275.

Herrmann, R.B., 1973. Some aspects of bandpass filtering of surface waves, *Bull. seism. Soc. Am.*, **63**, 663–671.

Herrmann, R.B., 1987. *Computer Programs for Seismology*, St Louis University, St Louis, MO.

Herron, E.M., 1972. Sea-floor spreading and the Cenozoic history of the East-Central Pacific, *Geol. Soc. Am. Bull.*, **83**, 1671–1691.

Hussong, D.M., Edwards, P.B., Johnson, S.H., Campbell, J.F. & Sutton, G.H., 1976. Crustal structure of the Peru–Chile trench 8°–12° latitude, in *The Geophysics of the Pacific Ocean Basin and its Margin*, Geophys. Monogr. Ser., **19**, pp. 71–85, eds Sutton, G., Manghnani, M. & Moberly, R., Am. geophys. Un., Washington, DC.

Larson, R.L., Pitman, W.C., Golovchenko, X., Cande, S.C., Dewey, J.F., Haxby, W.F. & LaBrecque, J.L., 1985. *The Bedrock Geology of the World* (*Map*), W.H. Freeman, New York.

Lewis, B.T.R., 1978. Evolution of ocean crust seismic velocities, *Ann. Rev. Earth planet. Sci.*, **6**, 377–404.

Mammerickx, J., Herron, E. & Dorman, L., 1980. Evidence for two fossil spreading ridges in the Southeast Pacific, *Geol. Soc. Am. Bull.*, **91**, 263–271.

Mitchell, B.J. & Yu, G.K., 1980. Surface wave dispersion, regionalized velocity models, and anisotropy of the Pacific crust and upper mantle, *Geophys. J.R. astr. Soc.*, **63**, 497–514.

Morgan, W.J., 1972. Plate motions and deep mantle convection, in *Studies in Earth and Space Sciences*, Geol. Soc. Am. Mem., **132**, 7–22, eds Shagam, R., Hargraves, R.B., Morgan, W.J., Van Houten, F.B., Burk, C.A., Holland, M.D. & Hollister, L.C., Geol. Soc. Am., Boulder, CO.

Nishimura, C. & Forsyth, D., 1988. Rayleigh wave phase velocities in the Pacific with implications for azimuthal anisotropy and lateral heterogeneities, *Geophys. J.R. astr. Soc.*, **94**, 479–501.

Nishimura, C. & Forsyth, D., 1989. The anisotropic structure of the upper mantle in the Pacific, *Geophys. J.*, **96**, 203–226.

Okal, E.A. & Cazenave, A., 1985. A model for the plate tectonic evolution of the east-central Pacific based on SEASAT investigations, *Earth planet. Sci. Lett.*, **72**, 99–116.

Pardo-Casas, F. & Molnar, P., 1987. Relative motion of the Nazca (Farallon) and South American plates since late Cretaceous time, *Tectonics*, **6**, 233–248.

Pilger, R.H., Jr. & Handschumacher, D.W., 1981. The fixed-hotspot hypothesis and origin of the Easter-Sala y Gomez-Nazca trace, *Geol. Soc. Am. Bull.*, **92**, 437–446.

Principal, P., 1974. A geophysical study of the Sala y Gomez Ridge, *MSc thesis*, University of Hawaii, Honolulu, Hawaii.

Rodi, W.L., Glover, P., Li, T.M.C. & Alexander, S.S., 1975. A fast, accurate method for computing group-velocity partial derivatives for Rayleigh and Love modes, *Bull. seism. Soc. Am.*, **65**, 1105–1114.

Russell, D.R., 1987. Multi-channel processing of dispersed surface waves, *PhD thesis*, St. Louis University, St. Louis, MO.

Russell, D.R., Herrmann, R.B. & Hwang, H.J., 1988. Application of frequency variable filters to surface wave amplitude analysis, *Bull. seism. Soc. Am.*, **78**, 339–354.

Sclater, J.G., Parsons, B. & Jaupart, C., 1981. Oceans and continents: similarities and differences in the mechanisms of heat loss, *J. geophys. Res.*, **86**, 11535–11552.

Sleep, N.H., 1992. Hotspots and mantle plumes, *Ann. Rev. Earth planet. Sci.*, **20**, 19–43.

Smith, M.L. & Dahlen, F.A., 1973. The azimuthal dependence of Love and Rayleigh wave propagation in a slightly anisotropic medium, *J. geophys. Res.*, **78**, 3321–3333.

Smith, W.H.F., 1990. Marine geophysical studies of seamounts in the Pacific ocean basin, *PhD thesis*, Columbia University, New York.

Spudich, P. & Orcutt, J., 1980. A new look at the seismic velocity structure of the oceanic crust, *Rev. Geophys. Space Phys.*, **18**, 627–645.

Stein, S. & Wiens, D.A., 1986. Depth determination for shallow teleseismic earthquakes: methods and results, *Rev. Geophys. Space Phys.*, **24**, 806–832.

Talandier, J. & Okal, E.A., 1987. Crustal structure in the Society and Tuamotu islands, French Polynesia, *Geophys. J.R. astr. Soc.*, **88**, 499–528.

Tryggvason, E., 1962. Crustal structure of the Iceland region from dispersion of surface waves, *Bull. seism. Soc. Am.*, **52**, 359–388.

U.S. Naval Oceanographic Office, 1985. *DBDB5 Bathymetric Data*, National Geophysical Data Center, Boulder, Colorado.

Wilson, J.T., 1963a. Hypothesis of Earth's behavior, *Nature*, **198**, 925–929.

Wilson, J.T., 1963b. Evidence from islands on the spreading of ocean floors, *Nature*, **197**, 536–538.

Wilson, J.T., 1963c. A possible origin of the Hawaiian Islands, *Can. J. Phys.*, **41**, 863–870.

Woods, M.T., Russell, D.R. & Herrmann, R.B., 1989. Dispersion of short period surface waves within the Ozark Uplift and Illinois Basin, *Seism. Res. Lett.*, **60**, 111–118.

Woods, M.T., Lévêque, J.-J., Okal, E.A. & Cara, M., 1991. Two-station measurements of Rayleigh wave group velocity along the Hawai'ian swell, *Geophys. Res. Lett.*, **18**, 105–108.

Wysession, M.E., Okal, E.A. & Miller, K.L., 1991. Intraplate seismicity of the Pacific basin, *Pure appl. Geophys.*, **135**, 261–359.

Yu, G.-K. & Mitchell, B., 1979. Regionalized shear velocity models of the Pacific upper mantle from observed Rayleigh and Love wave dispersion, *Geophys. J.R. astr. Soc.*, **57**, 311–342.

Zhang, Y.S. & Tanimoto, T., 1989. Three-dimensional modelling of upper mantle structure under the Pacific Ocean and surrounding area, *Geophys. J. Int.*, **98**, 255–269.

Zhang, Y.-S. & Tanimoto, T., 1991. Global Love wave phase velocity variation and its significance to plate tectonics, *Phys. Earth planet. Inter.*, **66**, 160–202.